PERGAMON

International Journal of Solids and Structures 39 (2002) 2435–2463

INTERNATIONAL JOURNAL OF SOLIDS and STRUCTURES

www.elsevier.com/locate/ijsolstr

An analytical delamination model for laminated plates including bridging effects

Fabrizio Greco *, Paolo Lonetti, Raffaele Zinno

Department of Structural Engineering, University of Calabria, 87030 Cosenza, Italy

Received 23 July 2001; received in revised form 28 January 2002

Abstract

A penalised interface model, whose strain energy is the penalty functional related to interface adhesion constraint, is introduced in conjunction with a damageable interface whose local constitutive law, in turn, represents bridging stress effects, in order to analyse delamination and bridging phenomena in laminated plates. The laminate is modelled by means of first-order shear deformable layer-wise kinematics and the governing equations are formulated in the form of a non-linear differential system with moving intermediate boundary conditions related to opportune delamination and bridging growth conditions. The problem is solved through an analytical approach. The model leads to an accurate and self-consistent evaluation of the energy release rate and its mode components due to the inclusion of significant contributions arising from coupling between in-plane and transverse shear stresses, and to an asymptotic estimate of interlaminar stresses. The salient features of the proposed model are investigated in the context of an energy balance approach and of a *J*-integral formulation, thus providing simple results useful to model delamination growth and bridging behaviour when mixed mode loading is involved. The accuracy of the proposed model is substantiated through comparisons with results from continuum analysis obtained by a finite element (FE) procedure. The effectiveness of the proposed model is highlighted by showing the solution of a two-layered plate scheme subjected to pure and mixed mode loading conditions and to fibre bridging stresses. The results point out that the present model, despite its low computational cost in comparison with more complex FE analyses, is an efficient tool to predict delamination and bridging evolution.

Keywords: Laminates; Delamination; Bridging; Interface elements

1. Introduction

The complete utilisation of fibre-reinforced laminates for civil, spacecraft, aircraft structure components or in the repair or rehabilitation of existing structures, is limited by their tendency to delaminate. As a matter of fact, laminated structures often exhibit initial delaminations arising from various causes such as technological imperfections, stress concentration, object impacts and global or local buckling of layers. Moreover, in rehabilitated structures delamination at the interface between the repairing composite

* Corresponding author. Tel.: +39-984-494-026; fax: +39-984-494-045.
E-mail address: f.greco@unical.it (F. Greco).

0020-7683/02/$ - see front matter
PII: S0020-7683(02)00118-X

laminate and the existing steel or concrete system may also occur as a failure mechanism. An appropriate modelling of the delamination phenomenon in this kind of structure, must take into account the parameters which govern the delamination behaviour like fracture toughness and the influence of bridging phenomena which may increase resistance to delamination and play an important role in delamination behaviour.

Due to anisotropy and non-homogeneity in toughness, a crack starting from these delaminations is often constrained to grow along the preferred interlaminar direction thus involving mixed mode conditions at the crack tip. Therefore, in order to accurately predict the growth of delamination when mixed mode loading is involved, some fracture criteria have been proposed, taking into account the experimental evidence of the different amount of energy required for mode I or mode II delamination (Hutchinson and Suo, 1992).

Published literature shows great interest both in mode I and mode II interlaminar fracture toughness testing (Robinson and Song, 1992) and in modelling delamination growth in composite systems (Storåkers and Andersson, 1988; Suo and Hutchinson, 1990; Schapery and Davidson, 1990; Suo, 1990; Cochelin and Potier-Ferry, 1991; Allix and Corigliano, 1996; Bruno and Greco, 2000, 2001a,b).

On the other hand, experimental evidence (Hwang and Han, 1989; Drzal and Madhukar, 1992) shows that bridging mechanisms, due to fibre crossover, through-the-thickness reinforcements and particle or grain bridging in polymer or ceramic matrix laminated composites, may provide a notable increase in fracture toughness as a delamination extends.

Through-the-thickness reinforcements, in the form of continuous or discontinuous stitches, may improve the fracture resistance of composites and are an efficient way to protect against delamination (Shu and Mai, 1993; Jain and Mai, 1994; Massabò and Cox, 1999).

Fibre crossover is due to fibres crossing the crack plane at a small angle as the delamination runs switching from one fibre–matrix interface to another (Suo et al., 1992), and provides closure tractions acting on the crack faces and shielding the crack tip, which diminish as the fibres are peeled out from the matrix. A softening two-parameter bridging law, which connects crack faces bridging tractions to displacement jumps across the interface, is able to represent the salient features of the phenomenon. It may depend on the frictional shear stresses between fibre and matrix which develop the matrix–fibre bonding, and on the number of crossover fibres per interface area unit. The bridging law can be obtained from micromechanical models or from experimental methods (Cox and Marshall, 1991; Bao and Song, 1993; Sørensen and Jacobsen, 1998).

An account of crack bridging concepts with reference to bridging modelling in the delamination of laminated composites can be found in Bao and Suo (1992): in this work mechanical properties which arise from inelastic processes associated with various bridging laws have been deduced and basic concepts related to large-scale bridging have been introduced. A fundamental point is that, when the bridged zone is not negligible in comparison with layer thickness or crack length in laminated composites, the resistance curve depends on specimen size and geometry and a stress analysis of the composite structure coupled with the bridging law must be performed.

Thus as the large-scale bridging condition prevails in composites, the analysis of bridging arising from fibre crossover or through-the-thickness reinforcement must be performed by using the bridging law concepts, the R-curve being no longer a material property.

In the present work a delamination analysis in layered plates which also includes the modelling of bridging stresses acting at the crack faces, is developed by utilising a refined laminated plate model. The laminate is divided in two sublaminates by interface elements which are able to simulate cohesive stresses and to accommodate stress singularities at the delamination front. The hypothesis of plane strain condition is assumed for sublaminates and its layers are supposed homogeneous orthotropic and linear elastic. A first-order shear deformable plate model is adopted for each sublaminate. In the undelaminated portion of the interface a penalised linear interface model, acting in the opening and sliding failure mode directions, is used to simulate the perfect adhesion between sublaminates. To impose interface adhesion constraint, the strain energy of the linear interface is treated as a penalty functional. The introduction of a penalised

interface, leads to a self-consistent method to evaluate energy release rates for mode I and mode II interlaminar crack advance. In fact, the energy release rates mode I and mode II components, are recovered in the penalty procedure from the interface strain energy aliquots related to opening and sliding displacement jumps, respectively. The above formulation also provides an estimate for interlaminar stresses which become singular at the delamination front, as the penalty parameter approaches infinity. Since interlaminar stresses are derived essentially from a plate model, the approximations in energy release rates evaluation obviously depend on the accuracy of the assumed plate model in representing the local crack tip strain state (Bruno and Greco, 2001b). For the applications here proposed, the first-order shear deformable plate theory is able to provide results of good accuracy as confirmed via finite element (FE) comparisons. The plate model can be eventually refined with more accurate plate theories, to improve the interlaminar stresses reconstruction in more complex laminate schemes.

The use of the first-order shear deformable plate theory allows a refined prediction of energy release rate components in comparison with classical delamination models, by modifying the singularity order of interlaminar crack tip stresses and accurately taking into account shear effects. In fact, the model includes coupling terms between shear and bending stress resultants in energy release rate, neglected in models frequently used in literature which adopt a single plate element to represent the undelaminated region of the laminate system. These terms may have a notable influence on energy release rate in composite laminated plate systems (Bruno and Greco, 2001a,b).

The inelastic processes related to the fibre bridging mechanism are taken into account by modelling bridging tractions acting at crack faces by means of a damageable interface introduced along the bridged zone. Softening two-parameter interface law with a maximum separation is used to simulate fibre crossover.

The governing equations are obtained through a variational procedure and constitute a non-linear differential system with moving intermediate boundary conditions. The moving boundary conditions related to delamination and bridging fronts are governed by opportune growth criteria. The delamination growth criterion is based on a mixed mode interlaminar fracture condition, whereas the growth of bridging fronts, related to normal and shear interlaminar bridging stresses, is assumed when limit separations are reached. The energy release rate modelling is investigated both in the context of an energy balance approach and of a J-integral formulation, obtaining analytical formulas for the energy release rates useful to highlight the role which an actual modelling of shear deformability plays in the delamination and bridging problem.

Analytical solutions are found for a two-layered plate loaded by end forces, and resistance curves are constructed to show the basic parameters affecting bridged delamination behaviour.

Comparisons with classical delamination models in which the use of the linear interface model is avoided by adopting a unique plate element in the undelaminated region, are carried out showing that the use of classical models provides a non-conservative prediction of the real delamination resistance of a layered system.

Moreover, the proposed approach is validated through comparisons with highly accurate results obtained by a two-dimensional (2D) FE analysis which utilises a non-linear incremental analysis strategy based on the arc length procedure. The comparisons are carried out for a simplified version of the interface constitutive law adopted for the analytical model. The numerical approach shows good agreement with the analytical model.

2. Delaminated plate model

The typical problem of a delaminated laminated plate sketched in Fig. 1 is analysed. The plate has length L, width B and contains a through-the-width plane delamination of length a whose front is aligned with the z-axis. The thickness of the two sublaminates separated by the delamination plane is h_1 and h_2 for the upper

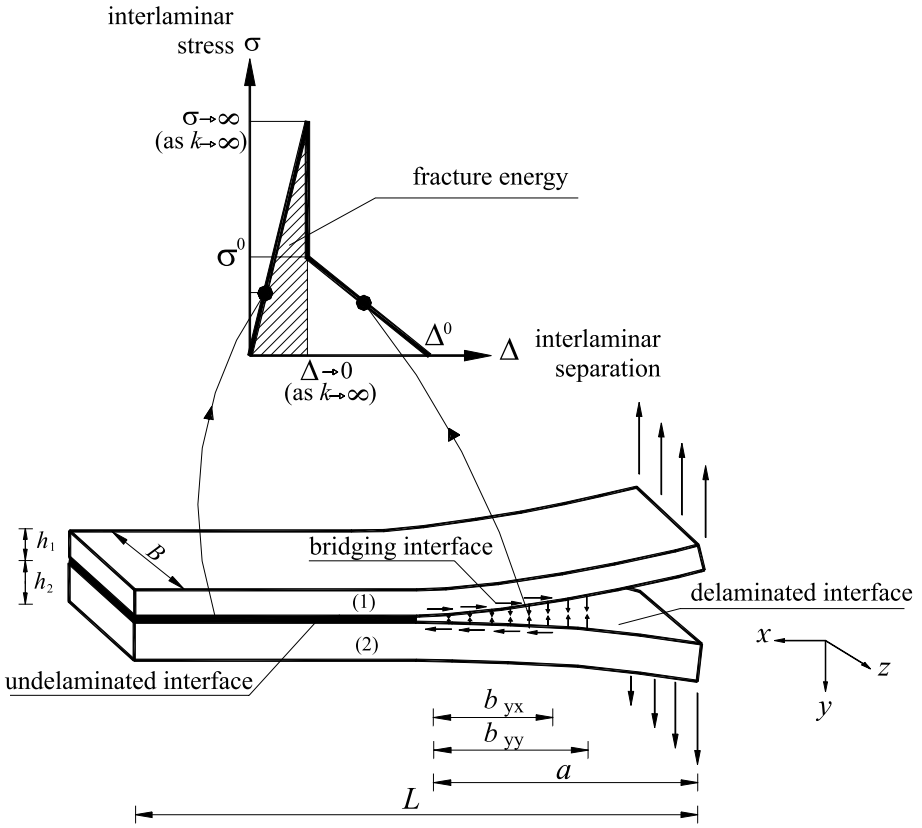

Fig. 1. Scheme of a laminated plate with a cohesive delamination.

and lower sublaminate, respectively. A damaged zone is assumed to be developed ahead of the delamination front in which opening and sliding bridging stresses act along lengths b_{yy} and b_{yx}, respectively. The delamination problem is modelled by considering the two sublaminates perfectly bonded along the interface containing the delamination except along the delamination length a where some bridging mechanisms may occur. The plane delamination is assumed to advance along the interface with its front parallel to the in-plane z-axes and plane strain condition in the x–y plane (or cylindrical bending) are supposed.

2.1. Interface model

Using a linear interface whose stiffness approaches infinity as a penalty parameter simulates perfect adhesion between layers along the undamaged interface. The linear interface has the following linear constitutive law which connects the traction vector $\boldsymbol{\sigma}$ acting at a generic point of the interface whose unit normal is coincident with the y-axis, with the relative interface displacement vector $\boldsymbol{\Delta}$,

$$\boldsymbol{\sigma} = k\boldsymbol{\Delta}, \tag{1}$$

where $\boldsymbol{\sigma}$ has components σ_{yy} and σ_{yx} in the normal (y) and tangential (x) directions, respectively, k is the stiffness coefficient of the interface, the components of $\boldsymbol{\Delta}$ are the relative displacement between the lower (2) and the upper (1) sublaminate, $\Delta u = u^2 - u^1$ and $\Delta w = w^2 - w^1$, in the normal (y) and tangential (x)

directions, respectively. The components of $\boldsymbol{\sigma}$ and $\boldsymbol{\Delta}$ are positive when aligned with the co-ordinate axes in Fig. 1.

Utilising the above linear interface allows the sublaminates to be connected along the interface and provides a self-consistent method to compute both total and individual mode components of energy release rate. As a matter of fact, the energy release rate mode components for crack advance within the interface are evaluated as the work of singular interlaminar stresses through the zeroing interface separations at the delamination front: this leads to the following formulas (Bao and Suo, 1992):

$$G_{\mathrm{I}} = \lim_{k\to\infty} \tfrac{1}{2} k\,\Delta w^2, \quad G_{\mathrm{II}} = \lim_{k\to\infty} \tfrac{1}{2} k\,\Delta u^2, \tag{2}$$

where subscript I, II denotes mode I, II components and Δu and Δw refer to the delamination front. Note that the mode I component G_{I} corresponds to opening transversal relative displacements at the crack tip $\Delta w > 0$ (no contact along the interface is allowed here).

The bridging mechanism is modelled by a non-linear interface whose normal and shear interlaminar stresses depend locally on the opening and sliding relative displacements across the damaged portion of the delamination, in the form

$$\boldsymbol{\sigma} = f(\boldsymbol{\Delta}), \tag{3}$$

where the same conventions previously adopted for the linear interface are assumed. In the following it is supposed that the bridging normal and shear tractions are derivable from a potential U, a function of the components of the relative interface displacement vector $\boldsymbol{\Delta}$, such that the following relations hold

$$\sigma = \frac{\partial U(\boldsymbol{\Delta})}{\partial \boldsymbol{\Delta}}, \quad U(\mathbf{0}) = 0, \tag{4}$$

where $\partial U(\boldsymbol{\Delta})/\partial \boldsymbol{\Delta}$, denotes a vector whose components on y and x axes are the derivative with respect to Δw and Δu, respectively.

Complex non-linear fibre bridging laws derived from different fibre bridging models, can be used (Spearing and Evans, 1992; Sørensen and Jacobsen, 1998; Iwamoto et al., 1999) but here the simple linear softening law is considered without affecting the salient aspects of the model. As a matter of fact, the main objective of this paper is to demonstrate a theoretical approach for an accurate delamination behaviour prediction.

Bridging stresses arising from fibre crossover can reasonably be simulated through the following two-parameter softening law:

$$\begin{cases} \sigma_{yy} = \sigma^0_{yy} - \frac{\sigma^0_{yy}}{\Delta w^0}\Delta w, & \text{if } \Delta w \leqslant \Delta w^0, \\ \sigma_{yy} = 0, & \text{if } \Delta w > \Delta w^0, \end{cases} \quad \begin{cases} \sigma_{yx} = \sigma^0_{yx}\frac{\Delta u}{|\Delta u|} - \frac{\sigma^0_{yx}}{\Delta u^0}\Delta u, & \text{if } |\Delta u| \leqslant \Delta u^0, \\ \sigma_{yx} = 0, & \text{if } |\Delta u| > \Delta u^0, \end{cases} \tag{5}$$

where Δw^0 and Δu^0 are the limit interface separations for normal and tangential interlaminar stresses, respectively. This constitutive law is decoupled in normal and tangential relative interface displacements and the directions of closure stresses are opposite to the separation displacements across the delamination. The potential defined in Eq. (4) assumes the form

$$U = U_{yx} + U_{yy}, \tag{6}$$

where

$$U_{yx} = \begin{cases} \sigma^0_{yx}|\Delta u| - \frac{\sigma^0_{yx}}{\Delta u^0}\frac{\Delta u^2}{2}, & |\Delta u| \leqslant \Delta u^0, \\ \sigma^0_{yx}\frac{\Delta u^0}{2}, & |\Delta u| > \Delta u^0, \end{cases} \quad U_{yy} = \begin{cases} \sigma^0_{yy}\Delta w - \frac{\sigma^0_{yy}}{\Delta w^0}\frac{\Delta w^2}{2}, & \Delta w \leqslant \Delta w^0, \\ \sigma^0_{yy}\frac{\Delta w^0}{2}, & \Delta w > \Delta w^0. \end{cases}$$

Note that the potential U has been extended over the entire delamination length although bridging stresses may operate only over the portions of the delamination length referred to as b_{yy} and b_{yx}. As far as the

problem of non-differentiability of U_{yx} is concerned, a perturbed regularising technique may be envisaged, in which the function $|\Delta u|$ is replaced by the following differentiable function

$$\begin{cases} |\Delta u| - \frac{\varepsilon}{2}, & \text{for } |\Delta u| > \varepsilon, \\ \frac{1}{2\varepsilon}|\Delta u|^2, & \text{for } |\Delta u| \leqslant \varepsilon, \end{cases} \tag{7}$$

approaching $|\Delta u|$ as $\varepsilon \to 0$.

Although the decoupling between opening and sliding bridging laws may correspond to a mathematical rather than physical model, this bridging response is able to provide a better understanding in delamination and bridging phenomena.

2.2. Laminate model

The two sublaminates separated by the delamination plane (see Fig. 2) are assumed to be made of unidirectional fibre-reinforced plies and each sublaminate is modelled by using a first-order shear deformable layer-wise kind of kinematics. Thus the following kinematics assumptions are used for the ith sublaminate ($i = 1, 2$):

$$\begin{cases} U_i(x_i, y_i) = u_i(x_i) + y_i\psi_i(x_i), \\ W_i(x_i, y_i) = w_i(x_i), \end{cases} \tag{8}$$

where the in-plane $U_i(x_i, y_i)$ and the transverse $W_i(x_i, y_i)$ displacements of the ith plate are expressed as functions of the corresponding midsurface in-plane and transverse displacements $u_i(x_i)$ and $w_i(x_i)$, respectively, and of section rotation $\psi_i(x_i)$.

The layers constituting the plates are assumed to be homogeneous, orthotropic and linearly elastic and the constitutive relations for each sublaminate are

$$\begin{Bmatrix} N_i \\ M_i \\ T_i \end{Bmatrix} = \begin{bmatrix} A_i & B_i & 0 \\ B_i & D_i & 0 \\ 0 & 0 & A_i^* \end{bmatrix} \begin{Bmatrix} u_i' \\ \psi_i' \\ \psi_i + w_i' \end{Bmatrix}, \quad i = 1, 2, \tag{9}$$

where the prime denotes the differentiation with respect the x_i co-ordinate; N_i, the in-plane stress resultant; M_i, the bending moment; T_i, the shear force; A_i, D_i, A_i^*, the standard axial, bending and shear stiffness, respectively; and B_i, the extension–bending stiffness. If the two sublaminates are made by specially orthotropic homogeneous plates stiffness terms specialise in the form

$$A_i = E_i h_i/(1 - v_i^{xz} v_i^{zx}), \quad D_i = E_i h_i^3/[12(1 - v_i^{xz} v_i^{zx})], \quad B_i = 0, \quad A_i^* = 5/6 G_i^{xy} h_i, \tag{10}$$

where E_i is the Young moduli along the x-axis; v_i^{xz}, v_i^{zx}, the Poisson's ratios along the x–z and z–x directions; G_i^{xy}, the shear modulus.

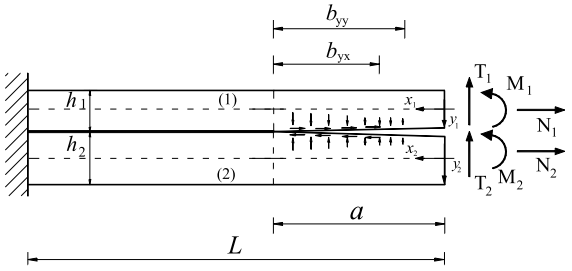

Fig. 2. Sublaminate configuration at a generic stage of delamination showing local co-ordinate systems and external loading.

3. Governing equations

Equilibrium equations at a generic stage of the quasi-static delamination and bridging growth, will be derived through the stationarity condition of a penalised total potential energy for unit width of the system sketched in Fig. 2, which assumes the form

$$\Pi_k(u_i, w_i, \psi_i) = \sum_{i=1}^{2} \int_0^L [\Phi_i(u_i, w_i, \psi_i)]\,\mathrm{d}x + \int_a^L \Lambda\,\mathrm{d}x + \int_0^a U\,\mathrm{d}x - \sum_{i=1}^{2} \boldsymbol{F}_i \cdot \boldsymbol{u}_i^0, \tag{11}$$

where Φ_i is the strain energy density of the ith sublaminate

$$\Phi_i(u_i, w_i, \psi_i) = \tfrac{1}{2}\Big[A_i u_i'^2 + 2B_i u_i' \psi_i' + A_i^* \big(\psi_i + w_i'\big)^2 + D_i \psi_i'^2\Big], \tag{12}$$

Λ indicates the strain energy of the undelaminated interface

$$\Lambda = \tfrac{1}{2} k\big(\Delta w^2 + \Delta u^2\big), \tag{13}$$

expressed in terms of the relative opening and sliding interface displacements

$$\begin{aligned} \Delta w(x) &= w_2(x) - w_1(x), \\ \Delta u(x) &= u_1(x) - \frac{h_1}{2}\psi_1(x) - \left[u_2(x) + \frac{h_2}{2}\psi_2(x)\right], \end{aligned} \tag{14}$$

the third integral is the energy dissipation of the bridging mechanism and the last term is the work done by the applied loads defined by the following relations

$$\boldsymbol{F}_i = \{-N_i, -M_i, -T_i\}^{\mathrm{T}}, \quad \boldsymbol{u}_i^0 = \{u_i(0), \psi_i(0), w_i(0)\}^{\mathrm{T}}. \tag{15}$$

Note that the strain energy of the linear interface assumes the form of a penalty functional which imposes the interface adhesion constraint, the interface stiffness k being the penalisation parameter. Moreover, in (11) the subscript k denotes dependence on the penalty parameter.

The first variation of (11) results in

$$\begin{aligned} &\sum_{i=1}^{2} \int_0^L \Big[N_i\,\delta u_i' + M_i\,\delta\psi_i' + T_i\,\delta\big(\psi_i + w_i'\big)\Big]\,\mathrm{d}x + k\int_a^L (\Delta w\,\delta\Delta w + \Delta u\,\delta\Delta u)\,\mathrm{d}x \\ &\quad + \int_0^a \big(\sigma_{yy}\,\delta\Delta w + \sigma_{yx}\,\delta\Delta u\big)\,\mathrm{d}x - \sum_{i=1}^{2} \boldsymbol{F}_i \cdot \delta\boldsymbol{u}_i^0 = 0, \end{aligned} \tag{16}$$

valid for every kinematically admissible displacements, and after integration by part furnishes the equilibrium equations together with the boundary and interior stress compatibility conditions at a generic stage of delamination evolution. Note that in this equilibrium configuration normal and tangential bridging tractions, expressed as a function of interface separations through Eq. (5), may act along different lengths b_{yy} and b_{yx}, respectively. The equilibrium solution satisfying (16) is not a minimum for the functional in Eq. (11) since the bridging potential U for the linear softening law considered here, is not a strictly convex function in the convex set $C = \{\Delta w > 0\}$, that is the following relation

$$U(\boldsymbol{\Delta}) - U(\bar{\boldsymbol{\Delta}}) - \frac{\partial U}{\partial \boldsymbol{\Delta}}(\bar{\boldsymbol{\Delta}})(\boldsymbol{\Delta} - \bar{\boldsymbol{\Delta}}) > 0 \quad \forall \boldsymbol{\Delta}, \bar{\boldsymbol{\Delta}} \in C \text{ with } \boldsymbol{\Delta} \neq \bar{\boldsymbol{\Delta}},$$

does not hold, and uniqueness is not in general to be expected. For different bridging laws characterised by a strictly convex potential the equilibrium solution is a minimum and uniqueness is guaranteed.

In deriving equilibrium equations, for convenience in later calculations and without affecting the generality of the analysis, assume that the sublaminates are symmetric about their midplane and have the same geometrical and mechanical properties (i.e. $A_1 = A_2 = A$, $D_1 = D_2 = D$, $B_1 = B_2 = 0$ and $A_1^* = A_2^* = A^*$). With these assumptions the boundary value problems governing relative opening and sliding interface displacements Δw and Δu, can be solved analytically. Obviously, generalisation to different sublaminates properties can be made without significant modifications, but the proposed equations are anyway able to show the main features of the delamination and bridging problem.

When the delamination leads to two sublaminates with different geometrical and mechanical properties, the governing equations become more complex and coupled in the opening and sliding interface displacements Δw and Δu. In principle, the problem admits an analytical solution similar to that of the simplified symmetric problem. The asymmetric delamination scheme should be useful, for example, to analyse the influence of residual stresses due to thermal effects. In this case free thermal strains should be introduced in constitutive relations (9), and in the total potential energy (11) the work of residual stresses should be included.

With clamped end condition for the whole laminate, equilibrium equations, boundary and interior compatibility conditions at common sections for stress resultants, respectively, for the opening interface separation function $\Delta w(x)$ can be put in the following form

$$\begin{cases} A^*(\Delta\psi' + \Delta w'') - 2\sigma_{yy} = 0, \\ A^*(\Delta\psi + \Delta w') - D\Delta\psi'' = 0, \end{cases} \quad \sigma_{yy} = \begin{cases} \sigma_{yy}^0 - \frac{\sigma_{yy}^0}{\Delta w^0}\Delta w, & 0 \leqslant x < b_{yy}, \\ k\,\Delta w, & b_{yy} \leqslant x < L - a + b_{yy}, \end{cases}$$

$$\begin{cases} \Delta w'(0) + \Delta\psi(0) = \frac{T_2 - T_1}{A^*}, & \Delta\psi'(0) = \frac{M_2 - M_1}{D}, \\ \Delta\psi(L - a + b_{yy}) = 0, & \Delta w(L - a + b_{yy}) = 0, \end{cases} \tag{17}$$

$$\begin{cases} \Delta w^-(b_{yy}) = \Delta w^+(b_{yy}), & \Delta\psi^-(b_{yy}) = \Delta\psi^+(b_{yy}), \\ \Delta\psi'^-(b_{yy}) = \Delta\psi'^+(b_{yy}), & \Delta w'^-(b_{yy}) + \Delta\psi^-(b_{yy}) = \Delta w'^+(b_{yy}) + \Delta\psi^+(b_{yy}), \end{cases}$$

where the origin of the x-axis is assumed to coincide with the right edge of the length b_{yy} along which normal bridging tractions act (see Fig. 3a), Δ has the usual meaning of difference between variables relative to the lower and upper sublaminate and superscripts $+$ or $-$ denote that the relevant function is evaluated at the delamination front $x = b_{yy}^+$ or $x = b_{yy}^-$, respectively. The stress resultants appearing in (17) are evaluated at the cross-sections located at the origin of the x-axis and the opening displacement along the bridged zone b_{yy} is assumed strictly positive.

Analogously, the sliding interface separation function defined as

$$\Delta u(x) = u_1 - u_2 + h/2(\psi_1 + \psi_2), \quad 0 \leqslant x \leqslant L - a + b_{yx},$$

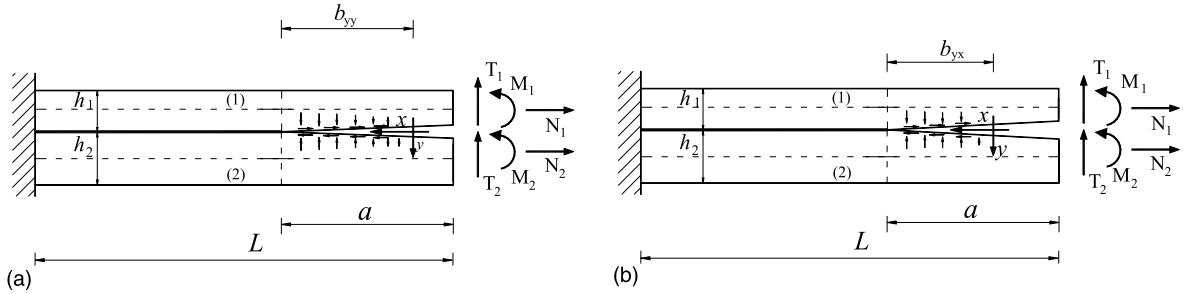

Fig. 3. Local co-ordinate system for (a) interface opening displacement function $\Delta w(x)$ and (b) interface sliding displacement function $\Delta u(x)$.

is governed by the following equations

$$A\,\Delta u'' - \sigma_{yx}\left(2+\frac{Ah^2}{2D}\right) - \frac{Ah}{2D}(T_1+T_2) = 0, \quad \sigma_{yx} = \begin{cases} \sigma^0_{yx}\frac{\Delta u}{|\Delta u|} - \frac{\sigma^0_{yx}}{\Delta u^0}\Delta u, & 0 \leqslant x < b_{yx}, \\ k\,\Delta u, & b_{yx} \leqslant x < L-a+b_{yx}, \end{cases}$$
$$\begin{cases} \Delta u'(0) = h\frac{M_2+M_1}{2D} + \frac{N_1-N_2}{A}, \\ \Delta u(L-a+b_{yx}) = 0, \end{cases} \quad \begin{cases} \Delta u^{-'}(b_{yx}) = \Delta u^{+'}(b_{yx}), \\ \Delta u^{-}(b_{yx}) = \Delta u^{+}(b_{yx}), \end{cases} \tag{18}$$

where, in this case, the origin of the x-axis is assumed to coincide with the right edge of the length b_{yx} along which tangential bridging tractions act (see Fig. 3b), superscripts + or − have the above introduced meaning and the stress resultants are evaluated at the cross-sections located at the origin of the x-axis. Note that the sum of shear resultants T_1 and T_2 is constant.

A complete kinematics description of the mode II variables is obtained by adding to Eq. (18) the following equation for the sum of sublaminate section rotations $\sum\psi = \psi_1 + \psi_2$:

$$D\sum\psi'' - (T_1+T_2) - \sigma_{yx}h = 0, \quad \sigma_{yx} = \begin{cases} \sigma^0_{yx}\frac{\Delta u}{|\Delta u|} - \frac{\sigma^0_{yx}}{\Delta u^0}\Delta u, & 0 \leqslant x < b_{yx}, \\ k\,\Delta u, & b_{yx} \leqslant x < L-a+b_{yx}, \end{cases}$$
$$\begin{cases} \sum\psi(L-a+b_{yx}) = 0, \\ \sum\psi'(0) = \frac{M_1+M_2}{D}, \end{cases} \quad \begin{cases} \Delta\psi^{-'}(b_{yx}) = \Delta\psi^{+'}(b_{yx}), \\ \Delta\psi^{-}(b_{yx}) = \Delta\psi^{+}(b_{yx}), \end{cases} \tag{19}$$

The limit for $k \to \infty$ of the sequence of solutions of the piecewise linear multipoint boundary value problem, decoupled in Δw and Δu, defined by Eqs. (17)–(19), furnishes equilibrium configurations at an intermediate stage of delamination evolution (i.e. for fixed delamination and bridging lengths). Eqs. (17) govern delamination evolution under mode I condition while Eqs. (18) and (19) refer to mode II condition. In numerical calculations k must be sufficiently large to enhance accuracy but relatively small to avoid badly conditioning of the problem.

The very high value of the interface stiffness coefficient k adopted in numerical calculations is of order 10^6 N/mm^3. Convergence studies performed, have shown that the above estimate for k is suitable to ensure accuracy of adhesion constraint and to avoid numerical instabilities. On the other hand, the choice of the interface stiffness could be made by means of physical considerations. As a matter of fact, the elastic interface with a large value of k is equivalent to an adhesive layer whose thickness is sufficiently small. Thus, within the common values for elastic moduli of composite materials, the adopted value for k corresponds to an equivalent layer thickness of about 10–20 times smaller than sublaminate thickness. More details about the problem of an optimal interface stiffness choice and of energy release rate convergence in the penalty procedure, can be found in Bruno and Greco (2001b).

Constructing the monotonic growth of delamination and bridging requires the following incremental growth conditions:

$$\begin{cases} G_{\mathrm{I}} + \lambda G_{\mathrm{II}} = G^{\mathrm{c}}_{\mathrm{I}}, & \delta a > 0, \\ \Delta w(0) = \Delta w^0, & \delta(a-b_{yy}) > 0, \\ \Delta u(0) = \Delta u^0, & \delta(a-b_{yx}) > 0, \end{cases} \tag{20}$$

where in the first equation, the delamination criterion, λ is a parameter calibrating the influence of mode II in the delamination criterion (Hutchinson and Suo, 1992), $G^{\mathrm{c}}_{\mathrm{I}}$ is the critical mode I fracture energy, the second and third equation is the opening and sliding bridging fronts propagation conditions, respectively, and δ denotes an infinitesimal increment in the relevant quantity.

4. Energy release rate modelling and fracture mechanics

In this section the energy release rates modelling is discussed by comparing the proposed interface approach, to fracture mechanics results. Within the fracture mechanics context, both the global energy balance (Griffith criterion) and the *J*-integral approach are taken into account emphasising the consistency between the present model and fracture mechanics theory. It will be shown that the considered global fracture mechanics approaches do not determine mode partition of energy release rate, whereas the proposed model provides a direct mode partition. On the other hand, the global methods are able to provide useful analytical formulas for the energy quantities governing the problem, in terms of stress resultant discontinuities.

For the delamination case without including bridging effects, the global energy approach was utilised in Bottega (1983) in a variational setting and in Storåkers and Andersson (1988) by a direct derivation of the potential energy, and was applied in Cochelin and Potier-Ferry (1991) by also introducing a modification due to the inclusion of shear terms arising from the Mindlin plate model. If a single plate is utilised to model the undelaminated portion of a laminate, as in the above cited references, also if accounting for shear deformability, the contribution of shear on energy release rate is generally small. Applying the energy approach to the present model, points out that the effects of shear deformability are captured in a more realistic way if a layer-wise kinematics model is adopted, since the local delamination tip strain state is better described.

The same conclusions are obtained with the *J*-integral approach (Suo et al., 1992) which will be applied to compute useful analytical formulas for the energy quantities involved in the analysis.

4.1. The global energy approach

With G representing energy release rate for unit surface, $\dot{a}$ the velocity of a point located at the delamination front, the point standing for partial differentiation in a time-like parameter, the energy balance at an intermediate stage of quasi-static monotonic delamination under dead loads is

$$G\dot{a} = -\frac{\mathrm{d}}{\mathrm{d}t}\Pi(u_i, w_i, \psi_i), \tag{21}$$

where $(\mathrm{d}/\mathrm{d}t)\Pi$ is the velocity of the total potential energy (11) evaluated along equilibrium solutions, in the limit for $k \to \infty$, namely

$$\Pi = \lim_{k\to\infty} \Pi_k. \tag{22}$$

The qualitative behaviour of strain energy and interlaminar stresses is shown in Fig. 4. The figure shows that the total potential energy contains a discontinuity point at the delamination front since in the limit $k \to \infty$ the linear interface strain energy density vanishes over the bonded interface length, $a < x \leqslant L$, except at the delamination front $x = a$, where it generally approaches to a finite value representing the energy release rate. This is due to the singular limit behaviour of the delamination front interlaminar stresses which, with exception for terms approaching infinity slower, approach infinity with the order $\mathrm{O}(k^{1/2})$ as $k \to \infty$, while the corresponding interlaminar separations Δu and Δw are of order $\mathrm{O}(k^{-1/2})$ within terms approaching zero slower (Bruno and Greco, 2001a,b). On the other hand, along the undelaminated interface ($a < x \leqslant L$) interlaminar stresses remain bounded while interface separations approach zero as $k \to \infty$.

Note that in the limit as $k \to \infty$ interlaminar stresses reconstruct the distributed Lagrange multipliers along $a < x \leqslant L$ and concentrated Lagrange multipliers at the delamination tip which reflect the singular behaviour of crack tip interlaminar stresses (see Fig. 5). Thus the external work in the total potential energy must include the contribution arising from point Lagrange multipliers applied at the delamination tip

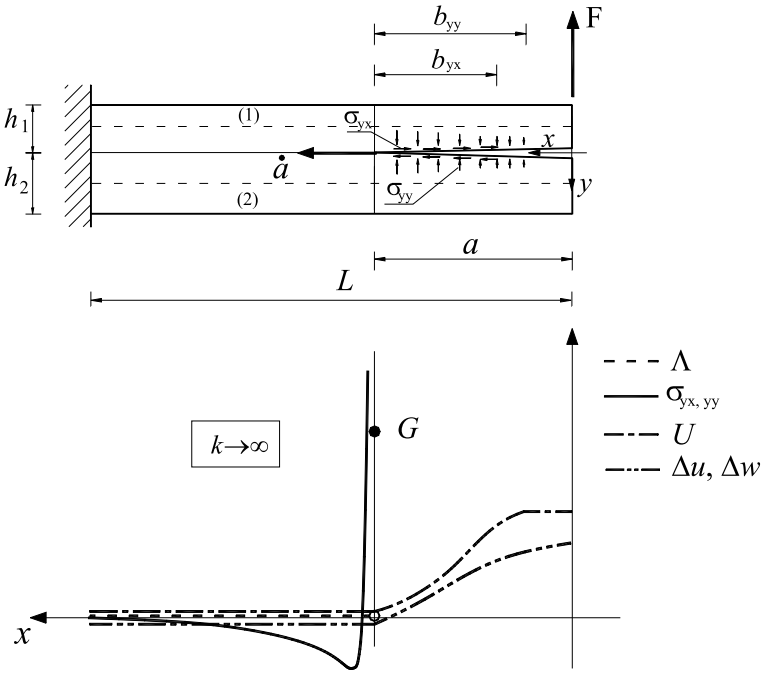

Fig. 4. Qualitative limit behaviour as $k \to \infty$ of interface strain energy density, interlaminar stresses, bridging potential and interface separations.

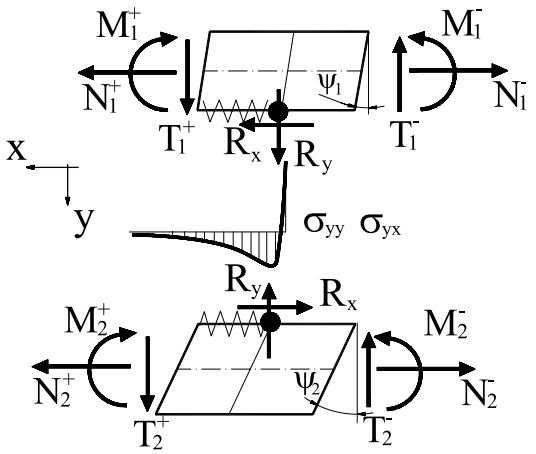

Fig. 5. Delamination front element: point Lagrange multipliers reflecting singular interlaminar stresses and section rotations.

$$\sum_{i=1}^{2} \boldsymbol{R}_i \cdot \boldsymbol{u}_i^{\mathrm{t}}, \tag{23}$$

where point Lagrange multipliers and displacement vectors at the delamination tip, are defined in Appendix A.

From (21) it follows that

$$G = \frac{1}{2}\sum_{i=1}^{2}\left[\!\left[N_i u_i' + M_i \psi_i' + \frac{T_i^2}{A_i^*} - 2T_i\psi_i \right]\!\right], \tag{24}$$

which specialises to

$$G = \frac{1}{2}\sum_{i=1}^{2}\left[\!\left[\frac{N_i^2}{A_i} + \frac{M_i^2}{D_i} + \frac{T_i^2}{A_i^*} - 2T_i\psi_i \right]\!\right], \tag{25}$$

when $B_i = 0$. The double bracket $[\![\cdot]\!]$ in Eqs. (24) and (25) indicates the jump of the enclosed quantity across a evaluated as $f^- - f^+$, namely the difference between the variable at $x = a^-$ and a^+. Details about analytical manipulations leading to Eqs. (24) and (25) can be found in Appendix A.

Alternatively, G can be evaluated by means of a penalised procedure as

$$G\dot{a} = \lim_{k\to\infty} -\frac{\mathrm{d}}{\mathrm{d}t}\Pi_k(u_i, w_i, \psi_i). \tag{26}$$

The main difference between the current procedure and the previous one is that in the penalised formulation (26) no stress discontinuity arises at the delamination front, since for finite values of k the adhesion constraint at the interface between the two sublaminates is not perfectly satisfied.

Similar arguments that conduced to Eq. (24) leads to

$$G = -\lim_{k\to\infty}[\![\Lambda + U]\!] = \lim_{k\to\infty}\left(\frac{1}{2}k\,\Delta w^2 + \frac{1}{2}k\,\Delta u^2\right), \tag{27}$$

which proves the connection between fracture mechanics and the interface approach. Details about the procedure based on Eq. (26) can be found in Appendix A.

It can be noted that G contains in addition to standard shear terms T_i^2/A_i^* coupling terms related to the quantity $T_i\psi_i$ which may have a notable influence in energy release rate (Bruno and Greco, 2001a). These terms do not appear in models currently used in literature (for an account of these models see, for instance, Allix and Corigliano (1996)) and shear effects are frequently circumscribed only to T_i^2/A_i^* terms. As a matter of fact, if the sublaminates are modelled as one plate element it is easy to show that equations formally equal to Eqs. (24) and (25) can be found: in this case, however, terms like $T_i\psi_i$ cancel each other due to the assumption of continuity of the section rotation ψ_i across the interface and due to equilibrium requirements.

Utilising the above energy balance during the monotonic advance of delamination leads to emphasising that the coupling terms arise from the delamination front localised discontinuity in stress resultants, which reflect the singular behaviour of interlaminar stresses, and emerge only when section rotation ψ_i is allowed to be discontinuous across the interface (see, for instance, Fig. 5).

4.2. The J-integral approach

Now we briefly follow an alternative route for delamination analysis: the J-integral approach. Let us consider the plate system in Fig. 6, the J-integral conservation provides

$$J(\Gamma_3) + J(\Gamma_2) = J_{\mathrm{ext}} - J_{\mathrm{b}} = G, \tag{28}$$

where J_{ext} is evaluated along any contour starting from the upper crack surface and ending on the lower crack surface enclosing the bridged zone which by virtue of path-independent properties is equal to $J(\Gamma_3)$ and J_{b} is the J-contribution of the bridging mechanism $J(\Gamma_2)$.

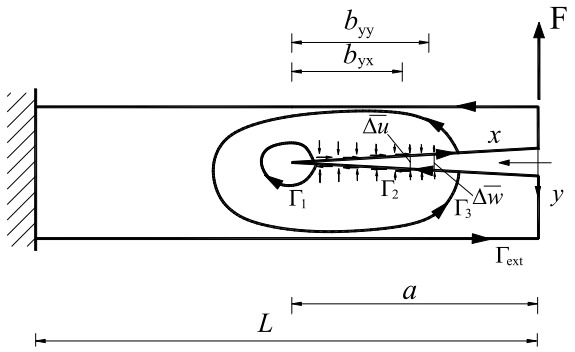

Fig. 6. Paths for J-integral evaluation in a bridged delaminated plate.

In Fig. 6, the segment Γ_1 has a vanishingly small radius and the corresponding path–integral represents the energy release rate available at the crack tip for crack advance with the minus sign $-G$, the segment Γ_2 runs along the upper and lower bridged crack surfaces $y = 0^+$ and 0^-, respectively, and the segment Γ_3 traverses the crack faces out of the bridging zones.

Evaluating the J-integral along a path like Γ_1 and Γ_3 with vertical segments behind and ahead of the delamination tip and with stresses and deformations of the proposed laminate model leads to

$$J = -\frac{1}{2}\int_{\Gamma}\left[\sigma_{xx}u' + \sigma_{xy}\left(w' + \psi\right)\right]\mathrm{d}y + \int_{\Gamma}\left[\sigma_{xy}\psi\right]\mathrm{d}y, \tag{29}$$

which for Γ_1 specialises to an energy release rate expression equal to that obtained in Eq. (24). Specific details about the previous J-integral application can be found in Appendix B.

Considering now the symmetric sublaminates case, the J-integral approach or, equivalently, the energy approach by appropriate definition of equivalent loading systems through Eqs. (17) and (18), are able to provide solutions for mode I and mode II energy release rates. Equivalent mode I and mode II loading systems are schematised in Fig. 7.

Applying (29) to the mode I scheme returns

$$\begin{aligned} J_{\mathrm{ext}} &= \frac{(M_1 - M_2)^2}{4D} + \frac{(T_1 - T_2)^2}{4A^*} + \frac{T_1 - T_2}{2}\Delta\psi(0) - \frac{M_{\mathrm{I}}^2}{D}, \\ J_{\mathrm{b}} &= \sigma^0_{yy}\Delta\bar{w} - \frac{\sigma^0_{yy}\Delta\bar{w}^2}{2\Delta w^0}, \\ G &= \frac{(M_1 - M_2)^2_{\mathrm{tip}}}{4D} + \frac{(T_1 - T_2)^2_{\mathrm{tip}}}{4A^*} + \frac{(T_1 - T_2)_{\mathrm{tip}}}{2}\Delta\psi(b_{yy}) - \frac{M_{\mathrm{I}}^2}{D}, \end{aligned} \tag{30}$$

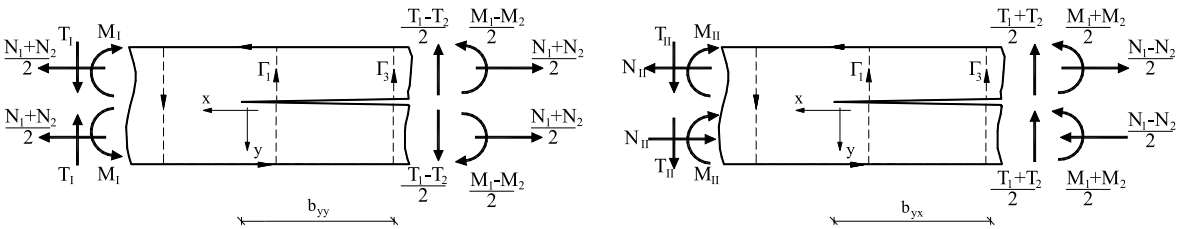

Fig. 7. Equivalent loading systems for mode I and mode II subproblems.

where $\Delta\psi(0)$ and $\Delta\psi(b_{yy})$ denote the relative rotation at the opening bridging and delamination front, respectively, and the subscript 'tip' indicates that the relevant quantity is taken at the delamination tip. Moreover, the vertical segment behind the delamination front is supposed at the clamped end and by continuity it can be noted that T_1 vanishes.

Analytical solutions for $L-a\to\infty$ (Bruno and Greco, 2001a) show that

$$\lim_{(L-a)\to\infty} G = \lim_{\substack{k\to\infty \\ (L-a)\to\infty}} \frac{1}{2}k\,\Delta w^2 = \frac{(M_1-M_2)^2_{\text{tip}}}{4D} + \frac{(T_1-T_2)^2_{\text{tip}}}{4A^*} + \frac{(T_1-T_2)_{\text{tip}}}{2}\frac{(M_1-M_2)_{\text{tip}}}{\sqrt{A^*D}}, \tag{31}$$

since the relative rotation $\Delta\psi(b_{yy})$ is $(M_1-M_2)_{\text{tip}}/(A^*D)^{1/2}$. The third term couples bending and shear resultants at the delamination tip and results in a notable effect since the ratio between the shear and coupling term is proportional to $Th/M(E_{xx}/G_{xy})^{1/2}$. Note that the proportionality factor may be less than unity because a high $(E_{xx}/G_{xy})^{1/2}$ ratio may be compensated by a very low Th/M value.

For the mode II scheme we have:

$$\begin{aligned} J_{\text{ext}} &= \frac{(M_1+M_2)^2}{4D} + \frac{(N_1-N_2)^2}{4A} + (T_1+T_2)[\psi(b_{yx})-\psi(0)] - \frac{N_{\text{II}}^2}{A} - \frac{M_{\text{II}}^2}{D}, \\ J_{\text{b}} &= \sigma^0_{yx}|\Delta\bar{u}| - \frac{\sigma^0_{yx}\,\Delta\bar{u}^2}{2\,\Delta u^0}, \\ G &= \frac{3(M_1+M_2)^2_{\text{tip}}}{16D} + \frac{(N_1-N_2)^2_{\text{tip}}}{16A} + \frac{3(M_1+M_2)_{\text{tip}}(N_1-N_2)_{\text{tip}}}{4Ah}. \end{aligned} \tag{32}$$

Note that no shear terms are contained in the energy release rate: this follows from antisymmetrical and equilibrium requirements. As a matter of fact the second term in (29) vanishes due to vertical equilibrium while the third term vanishes due to equilibrium and continuity of rotation across the interface.

The previous analysis has shown that, except for particular cases (i.e. symmetrical sublaminates), the energy and J-integral approaches do not separate energy release rate: to do this, a local post-processing of the equilibrium solution is needed and, for instance, the virtual crack closure method can be employed. We will not follow this kind of analysis since the objective here is to emphasise the effectiveness of the interface approach, which provides directly mode partition without the need of a post-processing.

5. Numerical solution procedure

The second-order boundary value problem defined by Eqs. (17) and (18), at a generic stage of delamination growth (i.e. for a fixed delamination length), defines a sequence of equilibrium configurations generated by the interface stiffness variation, and can be analytically solved by casting it in the form of a non-homogeneous first-order differential system:

$$\boldsymbol{y}_k' = \boldsymbol{F}_k\boldsymbol{y}_k + \boldsymbol{d}, \tag{33}$$

where the subscript k denotes explicit dependence on the penalty parameter k; $\boldsymbol{y}_k = \{\boldsymbol{y}^{\text{I}}, \boldsymbol{y}^{\text{II}}\}^{\text{T}}$ is a vector collecting in two subvectors $\boldsymbol{y}^{\text{I}}$ and $\boldsymbol{y}^{\text{II}}$, the displacement functions relative to mode I and mode II boundary value problems, respectively; $\boldsymbol{F}_k$ is the linear operator associated with the differential system and $\boldsymbol{d}$ is a non-linear vector.

Assume that during a load path the interface sliding displacement function does not change its sign along the sliding bridging length: with this hypothesis the system (33) can be solved as a linear system. The hypothesis is reasonable and will be justified in our examples. General solutions of (33) can be put in the form

$$\boldsymbol{y}_k = c_i\boldsymbol{u}_i e^{\lambda_i x}, \quad i = 1,\ldots,12, \tag{34}$$

where summation by repeated indices is implied and where $(\lambda_i, \boldsymbol{u}_i)$ are eigencouples of the eigenproblem

$$\boldsymbol{F}_k \boldsymbol{u} = \lambda_i \boldsymbol{u}.$$

The constants c_i appearing in Eq. (34) are extracted by using boundary and interior compatibility conditions contained in (17) and (18), which by using (33) result in the following linear system

$$\boldsymbol{B}_k \boldsymbol{c}_k = \boldsymbol{t}, \tag{35}$$

where the vector $\boldsymbol{c}_k$ collects the constants c_i, $\boldsymbol{B}_k$ is a matrix whose components contain an opportune combination of the components of the eigenvectors $\boldsymbol{u}_i$ and $\boldsymbol{t}_k$ is vector collecting boundary values. Details on the analytical solution of Eq. (33) can be found in Appendix C.

Due to the above analytical solution, delamination evolution in the laminated plate containing an initial defect a_0 can be numerically simulated by reducing the non-linear differential problem with moving boundary conditions to a non-linear algebraic system, which must be solved for a monotonic increase of the delamination length a. The monotonic increase of delamination length is obtained by finite increments Δa. The essential steps of the adopted incremental procedure are shown in Fig. 8, whereas specific details can be found in Appendix C.

6. Results and discussion

At first, delamination examples under pure mode I and mode II loading condition will be considered to point out the salient features involved in the delamination evolution problem. After, mixed-mode examples will be considered to show more realistic results. Comparisons between the classical delamination models and the proposed model show that the latter provides a more accurate resistance prediction in comparison to the former models: the better description of the local crack tip strain state, in fact, leads to capturing more realistically the effect of shear deformability on delamination growth behaviour. In the following numerical calculations, parameters are chosen in order to focus on the influence of the delamination model on delamination behaviour prediction.

6.1. Mode I case

In Fig. 9 resistance curves in terms of the conventional dimensionless energy release rate

$$\overline{G}_{\mathrm{I}} = \frac{G}{\sigma^0_{yy} \Delta w^0} = \frac{P^2 a^2}{\sigma^0_{yy} \Delta w^0 D},$$

namely evaluated without considering bridging and shear deformability, are plotted versus the delamination length a for a mode I delamination scheme loaded by two end forces for unit width P (the classical double cantilever beam scheme). The sublaminates are made of specially orthotropic homogeneous plates and the following geometrical and mechanical parameters are considered

$$h = 1.5 \text{ mm}, \quad E_x = 130,000 \text{ MPa}, \quad \nu_{xz}, \nu_{zx} = 0.15, \quad \sigma^0_{yy} = 5 \text{ MPa}, \quad Dw^0 = 0.05 \text{ mm},$$

which are assumed to be representative of a typical laminate subjected to fibre bridging (for order of magnitude of bridging law parameters see Bao and Suo (1992)). Two different values of the mode I critical energy release rate are considered to show the influence of the fracture energy on delamination analysis.

Three models are considered in Fig. 9: the proposed delamination model and two classical delamination models. According to the former (referred to as classical model 1 in Fig. 9) the undelaminated portion of the plate is modelled by means of a unique plate element and the laminate is considered as an assembly of three plates for which the Kirchhoff plate theory is adopted. The latter classical model (referred to as

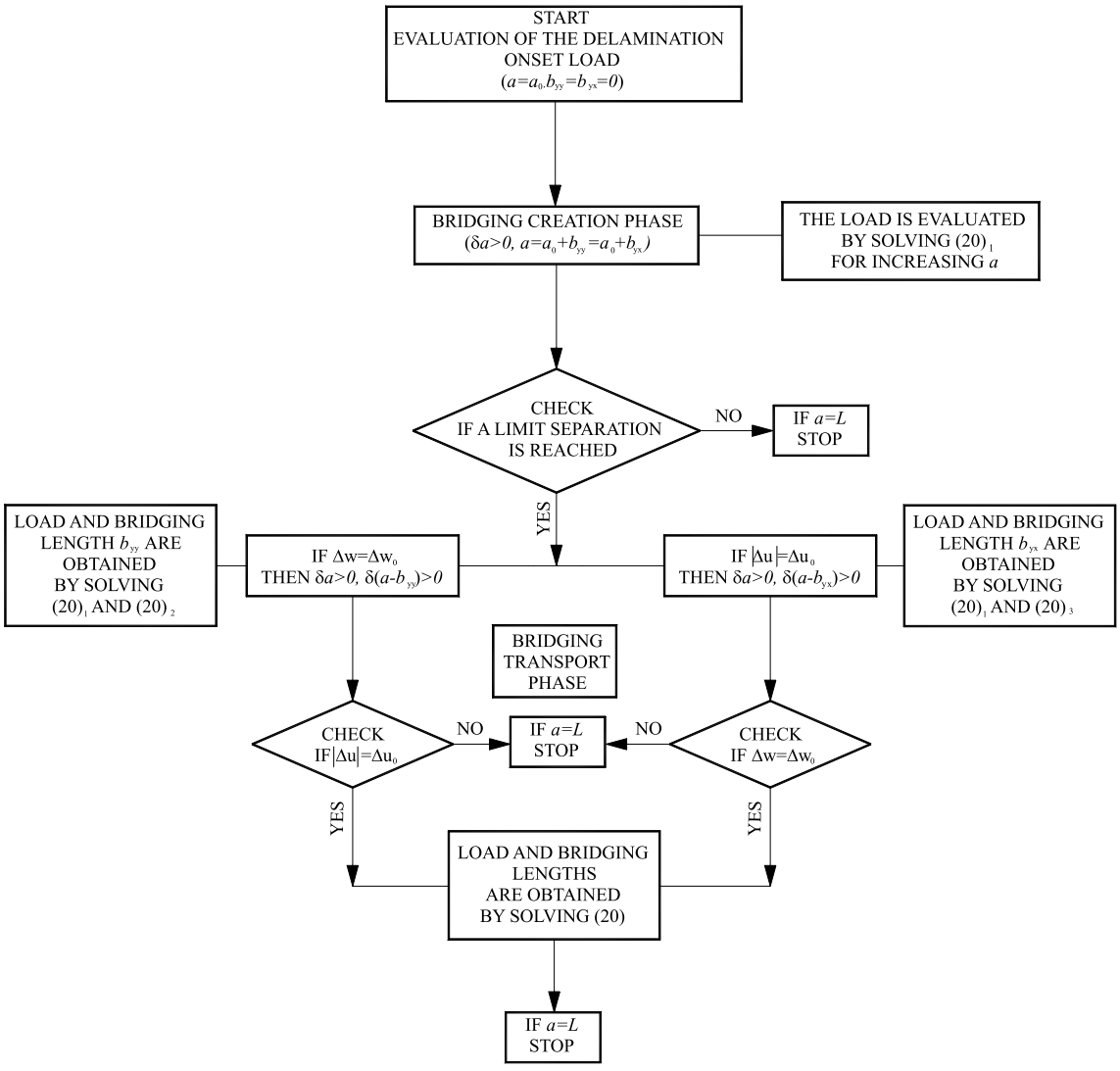

Fig. 8. Schematic drawing of the solution procedure.

classical model 2 in Fig. 9) includes shear deformability in the plate elements according to the Reissner–Mindlin kinematics. Bridging tractions acting along the delaminated region of the interface, are modelled by means of the softening two-parameter law introduced in Section 2.1.

In Fig. 9 the symbol 'I' denotes the initiation of the bridging creation phase (or initiation of delamination growth), while 'II' indicates that of the bridging transport phase. It can be noted that the classical delamination models approach to an asymptotic steady state resistance value at which bridging length practically propagates at a constant length:

$$\overline{G}_{\mathrm{I\,ss}} = \frac{G_{\mathrm{I}}^{\mathrm{c}}}{\sigma_{yy}^{0}\,\Delta w^{0}} + \frac{1}{2}. \tag{36}$$

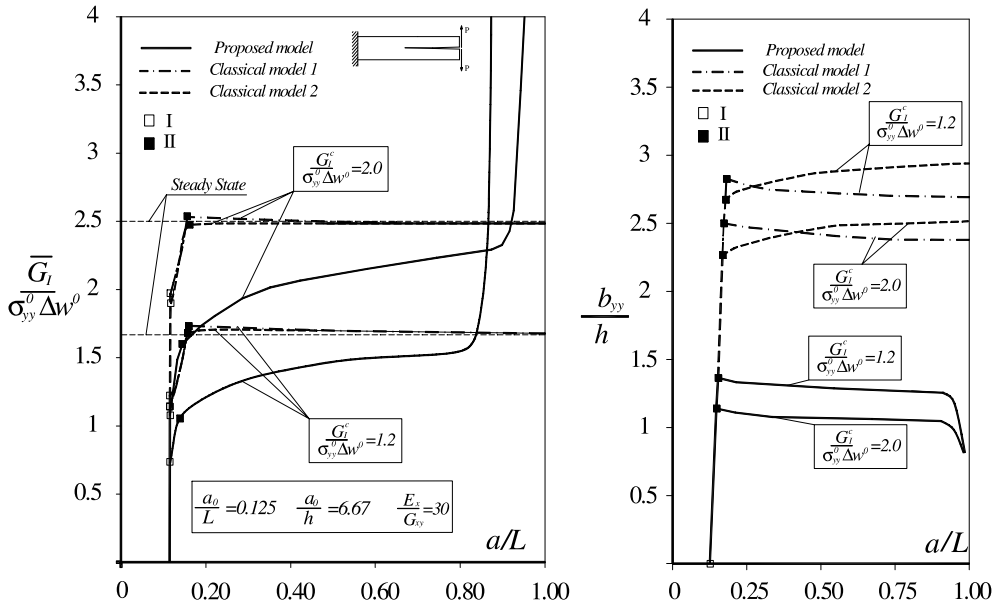

Fig. 9. Mode I example. Resistance and bridging curves as the delamination extends: comparison between the proposed model and the classical delamination models for different values of the fracture energy.

The steady state value in Eq. (36) is obtained by applying the J-integral as described in Section 4.2 to the classical delamination model without shear deformability, in the limit as the ratio between the delamination length and the bridging length a/b_{yy} approaches infinity. On the other hand, the proposed delamination model may approach a steady state asymptotically only if the laminate length is sufficiently long, but in proximity to clamped end a phenomenon of increase in resistance is shown. This can be ascribed to the effect of constrained warping of the transverse section which causes a decrease in energy release rate available for delamination growth.

In Fig. 9, near to the resistance curves, the corresponding bridging curves are plotted showing the evolution of bridging lengths as the delamination advances. From Fig. 9, the marked effect of shear deformability both on the load at the initiation of the bridging creation phase (I) and on the load at the beginning of bridging transport phase (II) can be noticed. As a matter of fact, bending–shear coupling terms play an important role in energy release rate evaluation and, consequently, on resistance curve providing a more accurate resistance prediction. This can be also noted from Eq. (30) which contain both pure and coupling shear terms. Moreover, resistance overestimation increases with the critical value of energy release rate $G_{\mathrm{I}}^{\mathrm{c}}$.

The comparison between the three models shows that the actual influence of shear deformability on delamination growth behaviour is captured only if the proposed delamination model is utilised. On the other hand, the use of a classical delamination model leads to an underestimate of the delamination resistance and the accuracy in delamination analysis is not largely increased also if shear deformability is accounted for (classical model 2).

6.2. Mode II case

A typical mode II scheme (the end loaded split) is considered in Fig. 10, where resistance curves in terms of the conventional dimensionless energy release rate

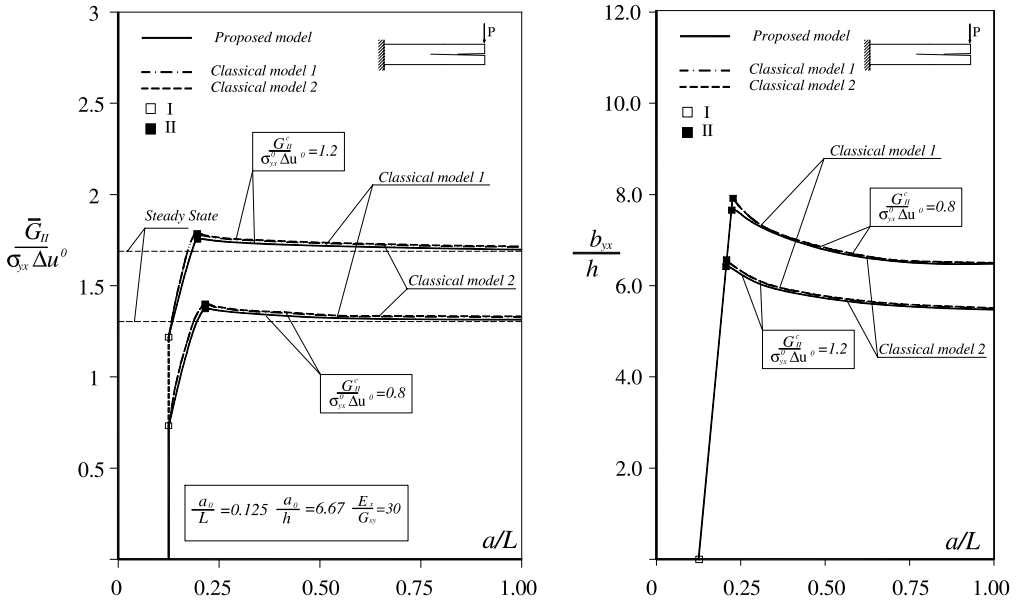

Fig. 10. Mode II example. Resistance and bridging curves as the delamination extends: comparison between the proposed model and the classical delamination models for different values of the fracture energy.

$$\overline{G}_{\mathrm{II}} = \frac{G}{\sigma^0_{yy}\,\Delta w^0} = \frac{3P^2a^2}{16\sigma^0_{yy}\,\Delta w^0 D},$$

are plotted versus the delamination length a together with the corresponding bridging curves. The following geometrical and mechanical parameters are considered

$$h = 1.5\ \text{mm}, \quad E_x = 130{,}000\ \text{MPa}, \quad v_{xz}, v_{zx} = 0.15, \quad \sigma^0_{yx} = 5\ \text{MPa}, \quad \Delta u^0 = 0.05\ \text{mm}.$$

As for the mode I case, two different values of the mode I critical energy release rate are considered to show the influence of the fracture energy on delamination analysis and the proposed model is compared to the classical delamination models. In Fig. 10 the meaning of classical model 1 and 2 is the same as that utilised in Fig. 9.

Since in this particular case the influence of shear deformability on delamination analysis is negligible as it is shown by Eq. (32), both the classical delamination and the proposed models tend towards the following asymptotic steady state resistance:

$$\overline{G}_{\mathrm{II\,ss}} = \frac{G^{\mathrm{c}}_{\mathrm{II}}}{\sigma^0_{yx}\,\Delta u^0} + \frac{1}{2}. \tag{37}$$

In this case, the resistance prediction obtained by the three models are practically the same and no resistance overprediction results.

6.3. Mixed mode case

In Fig. 11, a mixed mode example is considered. The asymmetric end loaded split scheme is considered and resistance curves in terms of the conventional global energy release rate

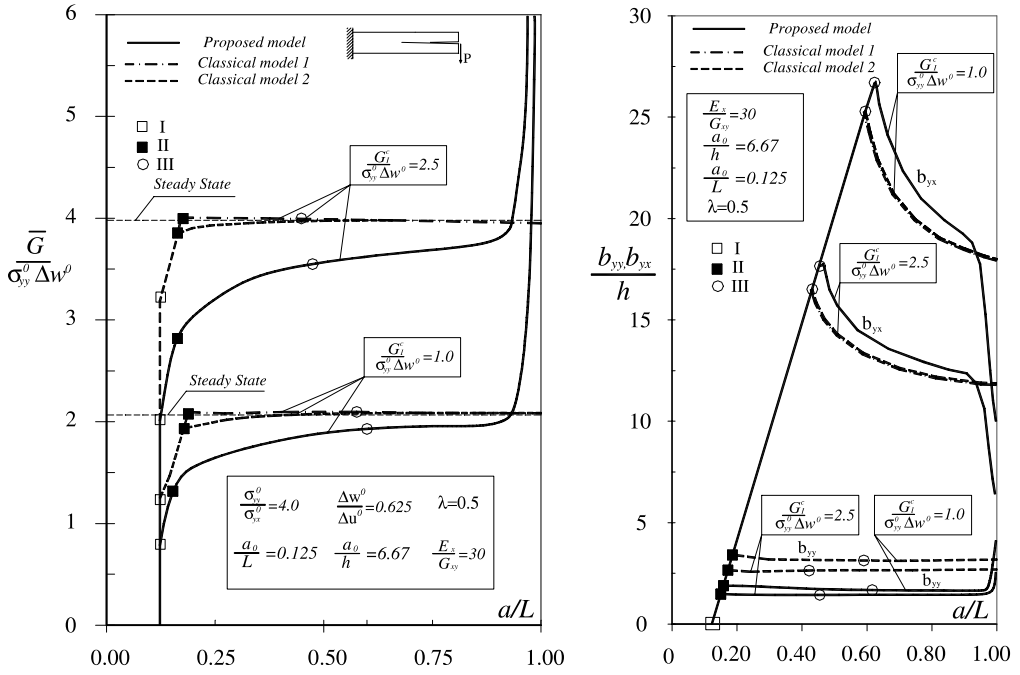

Fig. 11. Mixed mode example. Comparison between classical models and proposed delamination model in terms of resistance and bridging curves.

$$\overline{G} = \frac{G}{\sigma^0_{yy}\,\Delta w^0} = \frac{7P^2a^2}{16\sigma^0_{yy}\,\Delta w^0 D},$$

are plotted versus the delamination length. For the common geometrical and mechanical parameters, the same values utilised in the mode I case are considered, whereas the remaining values are shown in Fig. 11.

In Fig. 11, 'I' denotes the initiation of the bridging creation phase, 'II' and 'III' indicate the initiation of the normal and shear bridging transport phase, respectively. The classical delamination models approach to the following asymptotic steady state resistance:

$$\overline{G}_{\mathrm{ss}} = \frac{14}{11}\left(\frac{G^{\mathrm{I}}_{\mathrm{c}}}{\sigma^0_{yy}\,\Delta w^0} + \frac{1}{2} + \frac{1}{2}\lambda\frac{\sigma^0_{yx}\,\Delta u^0}{\sigma^0_{yy}\,\Delta w^0}\right). \tag{38}$$

Due to constrained warping, the proposed model shows an increase in resistance as in the mode I case, and no steady state is reached asymptotically. The bridging curves plotted near the resistance curves in Fig. 11, also confirm this. As in the mode I case, a notable overestimation in resistance prediction arises if classical delamination models are adopted, and the resistance overestimation increases with the critical value of energy release rate $G^{\mathrm{c}}_{\mathrm{I}}$. Both the classical delamination model (referred to as classical model 1) adopting the Kirchhoff plate theory and the classical delamination model (referred to as classical model 2) including shear deformability, are considered in Fig. 11. The inaccuracy in resistance prediction, is due to the notable underestimation in mode I energy release rate as it has been shown in Section 4: if a classical delamination model is utilised, in fact, shear effects are not actually captured.

7. Finite element validation

In order to validate the proposed model, comparisons with FE analyses based on a 2D continuum modelling, are proposed. The FE delamination analysis utilises 2D continuum plane strain elements and damage interface elements placed at the potential plane of interface debonding. Standard eight-node plane strain quadratic rectangular elements and 2D quadratic interface elements are used. Damage interface elements simulate the opening and sliding fracture modes by means of a three-parameter damage law (see Fig. 12). The constitutive law of interface elements for mode I (mode II) of fracture, defined in terms of the relative displacement at the interface, is assumed to be linear elastic until the stress reaches a threshold value σ^{t}_{yy} (σ^{t}_{yx}), then the stress is reduced linearly until the relative displacement reaches the failure value Δw^{0} (Δu^{0}). The relative opening displacement at which the material still behaves as linear elastic is ε^{I}_{0} (ε^{II}_{0}). Thus interface element constitutive relationship for mode I (mode II) is defined by means of the three parameters σ^{t}_{yy}, Δw^{0}, ε^{I}_{0} (σ^{t}_{yx}, Δu^{0}, ε^{II}_{0}). The softening portion of the damage interface law corresponds to the process zone of the bridging stresses.

The analytical delamination model generates various regularised models by choosing a finite value of the penalty parameter: thus by appropriate specialisation of the proposed interface model, which essentially is a four-parameter damage law, the FE damage model may be reproduced (Fig. 12). For the mode I case, the following relations can be used to specialise the analytical interface model to the FE damage model:

$$\sigma^{0}_{yy} = \sigma^{t}_{yy} + \frac{\sigma^{t}_{yy}}{\Delta w^{0} - \varepsilon^{I}_{0}}\varepsilon^{I}_{0}, \quad k = \frac{\sigma^{t}_{yy}}{\varepsilon^{I}_{0}}, \quad G_{I} = \frac{1}{2}k\varepsilon^{I^{2}}_{0},$$

and analogous relations can be utilised for the mode II case.

The numerical model utilises a non-linear incremental analysis strategy in which the arc length procedure (Crisfield, 1983) is adopted and convergence on the residual norm is selected. To follow the very unstable load deflection profile during progressive delamination, in the arc length procedure the root with the lowest residual force is selected. For the plane strain elements a fine integration scheme (3×3 G rule) is invoked and to avoid convergence difficulties, related to stress intensification near the delamination front, a sufficiently fine meshing is utilised. The FE computations were performed by using the FE code LUSAS, licensed from FEA Ltd.

The FE model is used here to analyse pure mode delamination examples, since for mixed mode cases the damage law of the numerical model is not able to reproduce the analytical interface model, the latter being uncoupled for the softening portion due to bridging and coupled for the elastic portion related to matrix

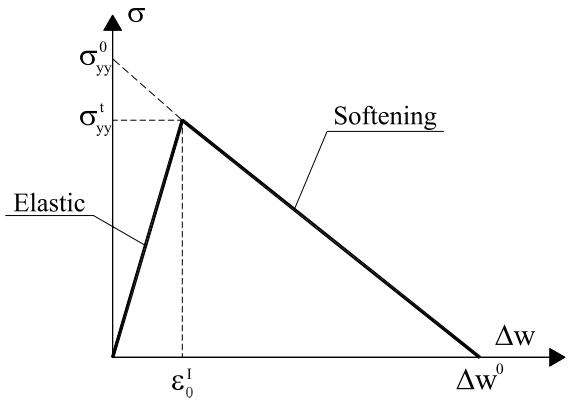

Fig. 12. Three-parameter delamination interface FE model: comparison with the proposed interface model.

failure. However it is reasonable to think that validation of the pure mode results obtained by the analytical model, are sufficient to substantiate the proposed model, the mixed mode case being derived, essentially, from superimposition of the pure mode cases.

At first the mode I loading case is considered by analysing a double cantilever scheme: note that the mode I case is a main point in substantiating the proposed model being strongly influenced by shear effects. Both deformed meshes of the delamination modelling, and the load–deflection graph for the FE model and the proposed model, are shown in Fig. 13. The following parameters were chosen for the analysis:

$$E_x = 130,000 \text{ MPa}, \quad v_{zx} = v_{xy} = v_{yz} = 0.15, \quad \sigma^{t}_{yy} = 30 \text{ MPa}, \quad \Delta w^0 = 0.05 \text{ mm}, \quad \varepsilon^{I}_0 = 0.002,$$
$$L = 70 \text{ mm}, \quad h = 1.5 \text{ mm}.$$

Fig. 13 shows a good agreement between the analytical and the FE model, confirming that the analytical model captures accurately the delamination growth behaviour. Furthermore, in Fig. 13 the undeformed mesh and two deformed meshes, corresponding to the initiation of the bridging creation phase (I) and of the bridging transport phase (II) respectively, are reported. Note that the phenomenon of increase in resistance shown by the analytical model is confirmed also by the FE model.

The same agreement is found in Fig. 14, where both mode I and mode II cases are considered in terms of load–delamination curves. The mode I case refers to a double cantilever scheme, whereas the mode II example to an end loaded split scheme. The following data are utilised:

$$E_x = 130,000 \text{ MPa}, \quad v_{zx} = v_{xy} = v_{yz} = 0.15, \quad \sigma^{t}_{yx} = \sigma^{t}_{yy} = 10 \text{ MPa}, \quad \Delta w^0 = \Delta u^0 = 0.01 \text{ mm},$$
$$\varepsilon^{I}_0 = \varepsilon^{II}_0 = 0.0056, \quad L = 70 \text{ mm}, \quad h = 1.5 \text{ mm}.$$

It is worth noting that the analysis developed by means of the FE model was very expensive with regard to computation time, due to the large number of evaluated load increments, whereas the analysis relative to the proposed analytical model requires a low computational cost.

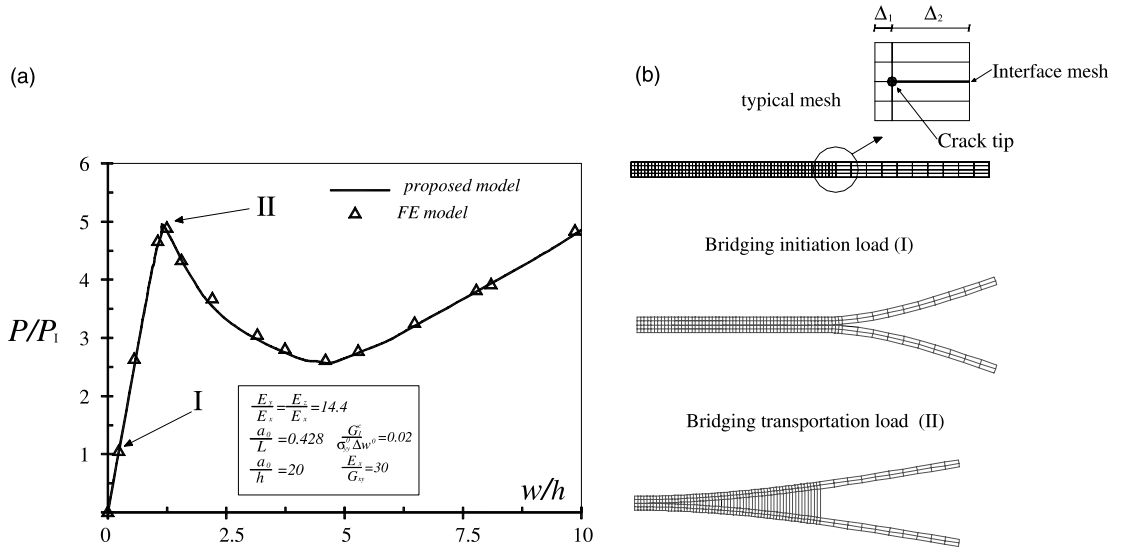

Fig. 13. (a) Load–deflection curves: comparison between analytical and FE model. (b) Typical undeformed mesh and deformed mesh at the initiation of the bridging creation (I), at the beginning of the bridging transportation phase (II). Details about meshing size are also shown.

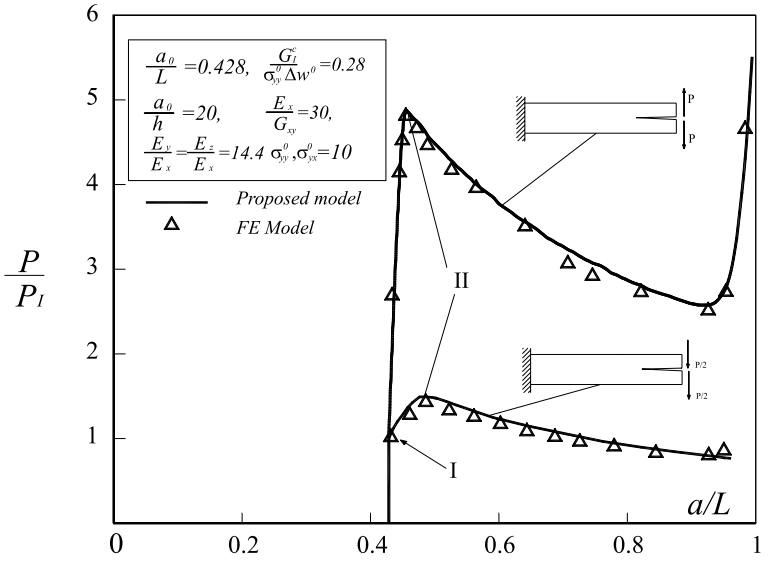

Fig. 14. Resistance curves: comparison between the proposed model and the FE model for mode I and mode II cases.

As a matter of fact, the FE non-linear analysis for the mode I case, took up to 30 min in evaluating 140 load increments, whereas the proposed analytical model took up to 5 min for 180 load increments of the delamination length. For the mode II case, the FE analysis took up to 25 min in evaluating 145 load increments, whereas the proposed model took up to 4 min for 180 load increments of the delamination length. The calculation were performed on a personal computer (CPU 600 MHz).

Moreover, the delamination model for both mode I and mode II cases utilises rectangular elements whose size Δ_1/h is equal to 0.44 along the initial undelaminated portion and of size Δ_2/h equal to 4 along the initial delaminated portion, where Δ_1 and Δ_2 are the lengths of the elements (see Fig. 13b). The 2D interface mesh uses 30 divisions as shown in Fig. 13b. Mesh refinement studies revealed that the above mesh discretisation is sufficiently fine to avoid convergence difficulties and to capture accurately stress behaviour near the delamination front.

8. Conclusions

An analytical approach, based on a first-order shear deformable layer-wise plate model in which interface elements are introduced to simulate delamination and fibre bridging stresses, is proposed to investigate the delamination behaviour of a laminated plate experiencing bridging effects. An initially penalised and subsequently damageable interface law introduces a cohesive delamination model which admits crack tip stress singularity, and provides a direct and self-consistent method to determine energy release rate and its mode partition. Governing equations, derived through a variational procedure, result in a non-linear differential system with moving intermediate boundary conditions, which must be solved in conjunction with appropriate delamination and bridging growth conditions. Under reasonable assumptions, an analytical solution procedure is proposed which reduces the delamination problem to a sequence of non-linear algebraic systems.

The relations between the proposed interface model and fracture mechanics are investigated through applications of the global energy balance and of the *J*-integral approach, pointing out the role which the plate model plays for an actual evaluation of the main quantities governing the problem.

Results obtained with reference to pure and mixed mode delamination and bridging examples, show that the proposed model, providing a better description of the local crack tip strain state, generates more accurate results in comparison with simplified delamination models widely used in literature. Comparisons with FE analyses utilising a 2D continuum formulation and damage interface elements, in fact, substantiate the accuracy of the present approach for a regularised version of the proposed interface model. Consequently, the analytical model here proposed, in spite of its low computational cost, is a useful tool to predict accurately the delamination and bridging behaviour of a laminated plate.

Finally, the main conclusion of the paper is that the analytical approach here proposed is able to capture effectively the interlaminar resistance behaviour of a laminated plate, avoiding the notable underestimation of the actual resistance obtained with simplified delamination models. Moreover, due to its analytical treatment, it provides a better understanding of some important aspects of the complex delamination and bridging problem, highlighting the main quantities affecting the interlaminar damage problem.

The paper is principally devoted to the calculation of resistance curve from a theoretical bridging law by using a refined delamination model. Nevertheless, if the inverse problem of bridging law evaluation from experimental resistance curve is considered, it is worth noting that the measure should be affected strongly by the adopted delamination model. This is particularly evident if the bridging law is evaluated by fitting the computed R-curves to measured R-curves: the bridging law parameters should be more accurate if evaluated by using the proposed model instead of a classical delamination model, since the proposed model provides a better prediction of interlaminar stresses through an accurate modelling of shear effects.

Although the analysis is referred here to one-dimensional delamination problems, thus allowing for an analytical treatment, results, in principle, can be extended, by using numerical solution methods, in cases where the delamination may have an arbitrary shape. In this context, the present analysis can be helpful to interpret more complex numerical approaches.

Appendix A

The point Lagrange multipliers (see Fig. 5) and displacement vectors at the delamination tip introduced in Eq. (23), are defined as

$$\begin{aligned} \boldsymbol{R}_1 &= \left\{R_x, R_y, R_x h_1/2\right\}^{\mathrm{T}}, & \boldsymbol{u}_1^{\mathrm{t}} &= \left\{u_1^{\mathrm{t}}, w_1^{\mathrm{t}}, \psi_1^{\mathrm{t}}\right\}^{\mathrm{T}}, \\ \boldsymbol{R}_2 &= \left\{-R_x, -R_y, R_x h_2/2\right\}^{\mathrm{T}}, & \boldsymbol{u}_2^{\mathrm{t}} &= \left\{u_2^{\mathrm{t}}, w_2^{\mathrm{t}}, \psi_2^{\mathrm{t}}\right\}^{\mathrm{T}}. \end{aligned} \tag{A.1}$$

Details about the procedure leading to Eqs. (24) and (25) are shown in the following. Using the standard rules for the time rate of an integral over the fixed region $R = [0, L]$ containing a moving discontinuity point p at $x = a$ with velocity $\dot{a}$,

$$\frac{\mathrm{d}}{\mathrm{d}t}\int_{R-a} f\,\mathrm{d}x = \int_{R-a} \dot{f}\,\mathrm{d}x + \dot{a}[\![f]\!],$$

where the double bracket $[\![\cdot]\!]$ indicates the jump of the enclosed quantity across p evaluated as $f^- - f^+$, namely the difference between the variable at $x = a^-$ and a^+, leads to the following expression for the time rate $(\mathrm{d}/\mathrm{d}t)\Pi$:

$$\begin{aligned} \frac{\mathrm{d}}{\mathrm{d}t}\Pi(u_i, w_i, \psi_i) = &\left[\sum_{i=1}^{2}\int_0^L \dot{\boldsymbol{\Phi}}_i\,\mathrm{d}x + \int_a^L \left(\sigma_{yy}\Delta\dot{w} + \sigma_{yx}\Delta\dot{u}\right)\mathrm{d}x + \int_0^a \dot{U}\,\mathrm{d}x - \sum_{i=1}^{2}\boldsymbol{F}_i\cdot\dot{\mathbf{u}}_i^0 - \sum_{i=1}^{2}\boldsymbol{R}_i\cdot\frac{\mathrm{d}}{\mathrm{d}t}\boldsymbol{u}_i^{\mathrm{t}}\right] \\ &+ \dot{a}\sum_{i=1}^{2}[\![\boldsymbol{\Phi}_i]\!]. \end{aligned} \tag{A.2}$$

In Eq. (A.2) the term in the square bracket denotes the fixed domain rate of the corresponding quantities while the remaining are the jumps in the flux over which strain energy densities are carried out across the point p. The second term in square bracket denotes the work of Lagrange multipliers σ_{yy}, σ_{yx} along the undelaminated interface. Note that jumps in the work of Lagrange multipliers and in bridging potential vanish: the former because it is zero at $x = a^+$, the latter due to the continuity of U which assumes zero value at the delamination front (see Eq. (4)).

The bracketed term in (A.2) is:

$$\sum_{i=1}^{2} \int_0^L \left[\left(A_i u_i' + B_i \psi_i' \right) \dot{u}_i' + \left(B_i u_i' + D_i \psi_i' \right) \dot{\psi}_i' + A_i^* (\psi_i + w_i')(\dot{\psi}_i + \dot{w}_i') \right] \mathrm{d}x + \int_a^L \left(\sigma_{yy} \Delta \dot{w} + \sigma_{yx} \Delta \dot{u} \right) \mathrm{d}x + \sum_{i=1}^{2} \left(N_i \dot{u}_i(0) + M_i \dot{\psi}_i(0) + T_i \dot{w}_i(0) \right) - \sum_{i=1}^{2} \boldsymbol{R}_i \cdot \frac{\mathrm{d}}{\mathrm{d}t} \boldsymbol{u}_i^{\mathrm{t}} \tag{A.3}$$

which after integration by part changes to

$$- \sum_{i=1}^{2} \int_0^L \left[N_i' \dot{u}_i + M_i' \dot{\psi}_i + T_i' \dot{w}_i - T_i \dot{\psi}_i \right] \mathrm{d}x + \int_a^L \left[\sigma_{yy} \Delta \dot{w} + \sigma_{yx} \Delta \dot{u} \right] \mathrm{d}x + \int_0^a \left(\sigma_{yy} \Delta \dot{w} + \sigma_{yx} \Delta \dot{u} \right) \mathrm{d}x + \sum_{i=1}^{2} [\![N_i \dot{u}_i + M_i \dot{\psi}_i + T_i \dot{w}_i]\!] - \sum_{i=1}^{2} \boldsymbol{R}_i \cdot \frac{\mathrm{d}}{\mathrm{d}t} \boldsymbol{u}_i^{\mathrm{t}} \tag{A.4}$$

with the aid of essential and natural boundary conditions.

Utilising equilibrium equations, interior stress resultants compatibility conditions and taking into account that common sections between plates coincide as delamination propagates, such that the following relations hold

$$\frac{\mathrm{d}}{\mathrm{d}t} u_1(a) = \frac{\mathrm{d}}{\mathrm{d}t} u_2(a), \quad \frac{\mathrm{d}}{\mathrm{d}t} w_1(a) = \frac{\mathrm{d}}{\mathrm{d}t} w_2(a), \quad \frac{\mathrm{d}}{\mathrm{d}t} \psi_1(a) = \frac{\mathrm{d}}{\mathrm{d}t} \psi_2(a), \tag{A.5}$$

the energy release rate is

$$G = \sum_{i=1}^{2} [\![- \Phi_i + N_i u_i' + M_i \psi_i' + T_i w_i']\!]. \tag{A.6}$$

In particular, interior stress resultant compatibility conditions are

$$\begin{array}{ll} [\![N_1]\!] = R_x, & [\![N_2]\!] = -R_x, \\ [\![T_1]\!] = R_y, & [\![T_2]\!] = -R_y, \\ [\![M_1]\!] = R_x h_1/2, & [\![M_2]\!] = R_x h_2/2. \end{array} \tag{A.7}$$

Obtaining Eq. (A.6) requires the following differentiation rule for a function at the delamination front

$$\frac{\mathrm{d}}{\mathrm{d}t} f(a,t) = \dot{f} + \dot{a} \frac{\partial}{\partial a} f. \tag{A.8}$$

After some manipulations from (A.6) Eqs. (24) and (25) are obtained.

The alternative procedure for the evaluation of G expressed by Eq. (26), is now considered in more contents. The explicit expression of the total potential energy Π_k appearing in Eq. (26) is

$$\frac{\mathrm{d}}{\mathrm{d}t} \Pi_k(u_i, w_i, \psi_i) = \left[\sum_{i=1}^{2} \int_0^L \dot{\Phi}_i \, \mathrm{d}x + \int_a^L \dot{\Lambda} \, \mathrm{d}x + \int_0^a \dot{U} \, \mathrm{d}x - \sum_{i=1}^{2} \boldsymbol{F}_i \cdot \dot{\boldsymbol{u}}_i^0 \right] + \dot{a} [\![\Lambda + U]\!]. \tag{A.9}$$

Note that in this case the two sublaminates are not perfectly connected along the interface for a finite value of k and consequently no stress resultants discontinuity arises at the delamination front. Thus the jumps in strain energy density and the work of delamination tip Lagrange multipliers are not present in Eq. (A.9). The jump in the strain energy of the undelaminated interface reduces only to the value of Λ at $x = a^+$ (with the minus sign), whereas the jump in bridging potential reduces to its value at $x = a^-$.

Consequently, using similar calculations that conduced to Eq. (A.6) leads to Eq. (27). Obtaining Eq. (27) considers that in the limit as k approaches infinity, the jump in U approaches to zero.

Appendix B

With reference to Fig. 6, evaluating the J-integral (Rice, 1968) along the closed path Γ which encloses an area free of singularities, leads to:

$$J(\Gamma) = \oint_{\Gamma} (Wn_x - t_i u_{i,x})\,\mathrm{d}s = J(\Gamma_1) + J(\Gamma_2) + J(\Gamma_3) = 0, \tag{B.1}$$

where W is the strain energy density; n_x, the x component of the unit exterior normal to the contour; t_i, the component of the traction vector acting on the surface whose trace in the x–y plane is Γ; $u_{i,x}$ stands for the partial derivative of the components of the displacement vector $\partial u_i/\partial x$; $\mathrm{d}s$, the differential arc length along Γ and summation is implied by repeated indices. Since $n_x = 0$ along the Γ_2 contribution

$$J(\Gamma_2) = -\int_{\Gamma_2} t_i u_{i,1}\,\mathrm{d}s = -\int_0^{\Delta\bar{w}} \sigma_{yy}\,\mathrm{d}(\Delta w) - \int_0^{\Delta\bar{u}} \sigma_{yx}\,\mathrm{d}(\Delta u), \tag{B.2}$$

with $\Delta\bar{w}$ and $\Delta\bar{u}$ are the separations at the end of the bridged surfaces. Thus, the J-integral conservation (B.1) provides Eq. (28).

If bridging stresses derive from a displacement potential U then

$$J_{\mathrm{b}} = U(\Delta\bar{w}, \Delta\bar{u}). \tag{B.3}$$

J_{b} is linked to the energy dissipation of the bridging mechanism introduced in (11) by

$$\frac{\mathrm{d}}{\mathrm{d}a}\int_0^a U\,\mathrm{d}x_1 = \int_0^a \frac{\partial}{\partial a} U\,\mathrm{d}x_1 + J_{\mathrm{b}}, \tag{B.4}$$

where total derivative $\mathrm{d}/\mathrm{d}a$ and partial derivative $\partial/\partial a$ by considerations about an eulerian reference system moving with the crack tip satisfy the following relation

$$\frac{\mathrm{d}}{\mathrm{d}a}() = \frac{\partial}{\partial a}() - \frac{\partial}{\partial x}().$$

When the bridging zone has a self-similar profile and a constant length during delamination advancing, a steady state large-scale bridging is reached and the J_{ext} becomes equal to the external energy release rate G_{ext} defined as

$$G_{\mathrm{ext}} = -\frac{\mathrm{d}}{\mathrm{d}a}\left\{ \sum_{i=1}^{4} \int_0^{\ell_i} [\Phi_i(u_i, w_i, \psi_i)]\,\mathrm{d}x_i + \int_0^{L-a} \Lambda\,\mathrm{d}x_3 - \sum_{i=1}^{2} \boldsymbol{F}_i \cdot \boldsymbol{u}_i^0 \right\},$$

since

$$G_{\mathrm{ext}} = J_{\mathrm{ext}} + \int_0^a \frac{\partial}{\partial a} U\,\mathrm{d}x_1, \tag{B.5}$$

and $\partial U/\partial a$ vanishes. Useful limit solutions can be obtained in a steady state case because J_{ext} does not depend on bridging law.

Appendix C

The mode I displacement function vector is

$$\boldsymbol{y}^{\mathrm{I}} = \left\{\Delta w^{(-)}, \Delta w'^{(-)}, \Delta\psi^{(-)}, \Delta\psi'^{(-)}, \Delta w^{(+)}, \Delta w'^{(+)}, \Delta\psi^{(+)}, \Delta\psi'^{(+)}\right\}^{\mathrm{T}}, \tag{C.1}$$

where, considering the same reference system introduced for Eq. (17), the superscripts $(-)$ and $(+)$ denote that the relevant functions are defined along the opening bridging zone and the bonded zone (i.e. $[0, b_{yy}]$ and $[b_{yy}, L-a+b_{yy}]$), respectively. The superscript T indicates transposition. Analogously, the mode II displacement function vector is

$$\boldsymbol{y}^{\mathrm{II}} = \left\{\Delta u^{(-)}, \Delta u'^{(-)}, \Delta u^{(+)}, \Delta u'^{(+)}\right\}^{\mathrm{T}}, \tag{C.2}$$

where with the same reference system introduced for Eq. (18), the superscripts $(-)$ and $(+)$ refer to the bridging sliding zone and bonded zone (i.e. $[0, b_{yx}]$ and $[b_{yx}, L-a+b_{yx}]$), respectively.

The linear operator $\boldsymbol{F}_k$ has the following matrix form:

$$\boldsymbol{F}_k = \begin{bmatrix} \boldsymbol{F}_{\mathrm{I}}^{(-)} & 0 & 0 & 0 \\ 0 & \boldsymbol{F}_{\mathrm{I}}^{(+)} & 0 & 0 \\ 0 & 0 & \boldsymbol{F}_{\mathrm{II}}^{(-)} & 0 \\ 0 & 0 & 0 & \boldsymbol{F}_{\mathrm{II}}^{(+)} \end{bmatrix}, \tag{C.3}$$

where

$$\boldsymbol{F}_{\mathrm{I}}^{(-)} = \begin{bmatrix} 0 & 1 & 0 & 0 \\ \frac{-2\sigma_{yy}^0}{\Delta w^0 A^*} & 0 & 0 & -1 \\ 0 & 0 & 0 & 1 \\ 0 & \frac{A^*}{D} & \frac{A^*}{D} & 0 \end{bmatrix}, \quad \boldsymbol{F}_{\mathrm{I}}^{(+)} = \begin{bmatrix} 0 & 1 & 0 & 0 \\ \frac{2k}{A^*} & 0 & 0 & -1 \\ 0 & 0 & 0 & 1 \\ 0 & \frac{A^*}{D} & \frac{A^*}{D} & 0 \end{bmatrix}, \quad \boldsymbol{F}_{\mathrm{II}}^{(-)} = \begin{bmatrix} 0 & 1 \\ \frac{-\sigma_{yx}^0}{\Delta u^0}\left(\frac{h^2}{2D}+\frac{2}{A}\right) & 0 \end{bmatrix},$$

$$\boldsymbol{F}_{\mathrm{II}}^{(+)} = \begin{bmatrix} 0 & 1 \\ k\left(\frac{h^2}{2D}+\frac{2}{A}\right) & 0 \end{bmatrix},$$

while $\boldsymbol{d}$ is

$$\left\{0, 2\sigma_{yy}^0/A^*, 0, 0, 0, 0, 0, 0, 0, \frac{h(T_1+T_2)}{2D} + \left(\frac{h^2}{2D}+\frac{2}{A}\right)\sigma_{yx}^0\frac{\Delta u}{|\Delta u|}, 0, \frac{h(T_1+T_2)}{2D}\right\}^{\mathrm{T}}. \tag{C.4}$$

Note that $\boldsymbol{d}$ depends non-linearly on the interface sliding displacement function.

The particular solution of (33) assumes the form

$$\bar{\mathbf{y}}_k = \left\{\Delta w_0, 0, 0, 0, 0, 0, 0, 0, 0, \Delta u_0\left[\frac{\Delta u}{|\Delta u|} + \frac{T_1+T_2}{2\sigma_{yx}^0\left(h+\frac{2D}{Ah}\right)}\right], 0, -\frac{h(T_1+T_2)}{k\left(h^2+\frac{4D}{A}\right)}, 0\right\}^{\mathrm{T}}. \tag{C.5}$$

The matrix of boundary conditions $\boldsymbol{B}$ assumes the following form:

$$\boldsymbol{B}_k = \begin{bmatrix} \boldsymbol{B}_{\mathrm{I}(1)} & \boldsymbol{B}_{\mathrm{I}(12)} & 0 & 0 \\ \boldsymbol{B}_{\mathrm{I}(21)} & \boldsymbol{B}_{\mathrm{I}(2)} & 0 & 0 \\ 0 & 0 & \boldsymbol{B}_{\mathrm{II}(1)} & \boldsymbol{B}_{\mathrm{II}(12)} \\ 0 & 0 & \boldsymbol{B}_{\mathrm{II}(21)} & \boldsymbol{B}_{\mathrm{II}(2)} \end{bmatrix},$$

where

$$\boldsymbol{B}_{\mathrm{I}(1)} = \begin{bmatrix} U_{11}\mathrm{e}^{\lambda_1 b_{yy}} & U_{21}\mathrm{e}^{\lambda_2 b_{yy}} & U_{31}\mathrm{e}^{\lambda_3 b_{yy}} & U_{41}\mathrm{e}^{\lambda_4 b_{yy}} \\ U_{12}+U_{13} & U_{22}+U_{23} & U_{32}+U_{33} & U_{42}+U_{43} \\ U_{14} & U_{24} & U_{34} & U_{44} \\ 0 & 0 & 0 & 0 \end{bmatrix},$$

$$\boldsymbol{B}_{\mathrm{I}(2)} = \begin{bmatrix} U_{57}\mathrm{e}^{\lambda_5(L-a)} & U_{67}\mathrm{e}^{\lambda_6(L-a)} & U_{77}\mathrm{e}^{\lambda_7(L-a)} & U_{87}\mathrm{e}^{\lambda_8(L-a)} \\ -U_{57} & -U_{67} & -U_{77} & -U_{87} \\ -U_{58} & -U_{68} & -U_{78} & -U_{88} \\ -U_{56}-U_{57} & -U_{66}-U_{67} & -U_{76}-U_{77} & -U_{86}-U_{87} \end{bmatrix},$$

$$\boldsymbol{B}_{\mathrm{I}(12)} = \begin{bmatrix} -U_{55} & -U_{65} & -U_{75} & -U_{85} \\ 0 & 0 & 0 & 0 \\ 0 & 0 & 0 & 0 \\ U_{55}\mathrm{e}^{\lambda_5(L-a)} & U_{65}\mathrm{e}^{\lambda_6(L-a)} & U_{75}\mathrm{e}^{\lambda_7(L-a)} & U_{85}\mathrm{e}^{\lambda_8(L-a)} \end{bmatrix},$$

$$\boldsymbol{B}_{\mathrm{I}(21)} = \begin{bmatrix} 0 & 0 & 0 & 0 \\ U_{13}\mathrm{e}^{\lambda_1 b_{yy}} & U_{23}\mathrm{e}^{\lambda_2 b_{yy}} & U_{33}\mathrm{e}^{\lambda_3 b_{yy}} & U_{43}\mathrm{e}^{\lambda_4 b_{yy}} \\ U_{14}\mathrm{e}^{\lambda_1 b_{yy}} & U_{24}\mathrm{e}^{\lambda_2 b_{yy}} & U_{34}\mathrm{e}^{\lambda_3 b_{yy}} & U_{44}\mathrm{e}^{\lambda_4 b_{yy}} \\ (U_{12}+U_{13})\mathrm{e}^{\lambda_1 b_{yy}} & (U_{22}+U_{23})\mathrm{e}^{\lambda_2 b_{yy}} & (U_{32}+U_{33})\mathrm{e}^{\lambda_3 b_{yy}} & (U_{42}+U_{43})\mathrm{e}^{\lambda_4 b_{yy}} \end{bmatrix},$$

$$\boldsymbol{B}_{\mathrm{II}(1)} = \begin{bmatrix} U_{910} & U_{1010} \\ U_{910}\mathrm{e}^{\lambda_9 b_{yx}} & U_{1010}\mathrm{e}^{\lambda_{10} b_{yx}} \end{bmatrix},$$

$$\boldsymbol{B}_{\mathrm{II}(2)} = \begin{bmatrix} -U_{1111} & -U_{1211} \\ U_{1112}\mathrm{e}^{\lambda_{11}(L-a)} & U_{1212}\mathrm{e}^{\lambda_{11}(L-a)} \end{bmatrix},$$

$$\boldsymbol{B}_{\mathrm{II}(12)} = \begin{bmatrix} 0 & 0 \\ -U_{1112} & -U_{1212} \end{bmatrix},$$

$$\boldsymbol{B}_{\mathrm{II}(21)} = \begin{bmatrix} U_{99}\mathrm{e}^{\lambda_9 b_{yx}} & U_{109}\mathrm{e}^{\lambda_{10} b_{yx}} \\ 0 & 0 \end{bmatrix},$$

where U_{ij} indicates the ith component of the jth eigenvector $\boldsymbol{u}_j$. Note that exponential functions for each mode problem appearing in Eq. (34) refer to two internal reference systems with origins placed at the fronts of opening or sliding bridging zone and at the delamination front, respectively.

The vector of boundary values $\boldsymbol{t}$ is

$$\boldsymbol{t} = \left\{ -\Delta w_0, \frac{T_2-T_1}{A^*}, \frac{M_2-M_1}{D}, 0,0,0,0,0, h\frac{M_2+M_1}{2D} + \frac{N_1-N_2}{A}, 0 \right.$$
$$\left. -\Delta u_0 \left[\frac{\Delta u}{|\Delta u|} + \frac{T_1+T_2}{2\sigma^0_{yx}\left(h+\frac{2D}{Ah}\right)} \right] - \frac{h(T_1+T_2)}{k\left(h^2+\frac{4D}{A}\right)}, \frac{h(T_1+T_2)}{k\left(h^2+\frac{4D}{A}\right)} \right\}^{\mathrm{T}}.$$

Using the above solution and noting (2) leads to observing that the opening and sliding interface separations and, consequently, energy release rate mode components during the monotonic advance of delamination depend, respectively, on

$$\begin{aligned} &\Delta w_k = y_5(0) = \Delta w_k\big(P, b_{yy}, a\big), \quad \Delta u_k = y_{11}(0) = \Delta u_k\big(P, b_{yx}, a\big), \\ &G_{\mathrm{I}} = G_{\mathrm{I}}\big(P, b_{yy}, a\big), \quad G_{\mathrm{II}} = G_{\mathrm{II}}\big(P, b_{yx}, a\big), \end{aligned} \tag{C.6}$$

where P denotes a load parameter, the subscript k indicates a sequence of functions and the energy release rates are evaluated by the limit values of these sequences.

The solution procedure adopted to solve the equations governing the delamination evolution is now described in specific details.

After evaluation of the load at the onset of delamination (with $b_{yy} = b_{yx} = 0$ and $a = a_0$) by solving the first term of the non-linear Eq. (20) which contains P as the only unknown, the solution procedure follows two phases: the bridging formation phase (which coincides with the initiation of delamination growth) and the bridging transport phase.

In the former bridging tractions appear but the origin of bridging zones remain fixed and, consequently, bridging lengths are equals: the load is evaluated by solving the first term of Eq. (20) for increasing delamination length (i.e. $\delta a > 0$, $a = a_0 + b_{yy} = a + b_{yx}$).

The latter begins when a limit separation condition (i.e. $|\Delta u| = \Delta u^0$ or $\Delta w = \Delta w^0$) at the bridging front is satisfied and both the delamination front (i.e. $\delta a > 0$) and opening or sliding bridging fronts (i.e., $\delta(a - b_{yy}) > 0$ or $\delta(a - b_{yx}) > 0$, respectively) propagate according if the opening or sliding limit separation is reached, respectively. During this phase the load and the opening or sliding bridging lengths are obtained by solving the first and second equations of the system (20) or the first and third equations of the system (20), respectively.

For example, if the opening limit separation is first reached, the opening bridging zone propagates together with delamination ($\delta(a - b_{yy}) > 0$ and $\delta a > 0$), while the sliding bridging zone is not transported (i.e. $\delta(a - b_{yx}) = 0$ and $b_{yx} = a - a_0$) and P and b_{yy} are extracted by the first and second equations of the system (20).

Afterwards, it may happen that increasing the delamination length leads to reaching the other limit separation at the bridging front which has not yet been transported: in this case bridging lengths b_{yx}, b_{yy} and the load are obtained by solving the entire system (20).

Alternatively, it may happen that the plate reaches complete delamination (i.e. $a = L$) without reaching a second limit separation.

Using a standard search procedure based on a modified Newton method solves the non-linear algebraic system arising during delamination growth.

References

Allix, O., Corigliano, A., 1996. Modelling and simulation of crack propagation in mixed-modes interlaminar fracture specimens. Int. J. Fract. 77, 111–140.

Bao, G., Song, Y., 1993. Crack bridging for fiber composites with slip-dependent interfaces. J. Mech. Phys. Solids 41, 1425–1444.

Bao, G., Suo, Z., 1992. Remarks on crack bridging concepts. Appl. Mech. Rev. 24, 355–366.

Bottega, W.J., 1983. A growth law for propagation of arbitrary shaped delaminations in layered plates. Int. J. Solids Struct. 19 (11), 1009–1017.

Bruno, D., Greco, F., 2000. An asymptotic analysis of delamination buckling and growth in layered plates. Int. J. Solids Struct. 37, 6239–6276.

Bruno, D., Greco, F., 2001a. Delamination in composite plates: influence of shear deformability on interfacial debonding. Cement Concr. Compos. 23 (1), 33–45.

Bruno, D., Greco, F., 2001b. Mixed mode delamination in plates: a refined approach. Int. J. Solids Struct. 38/50-51, 9149–9177.

Cochelin, B., Potier-Ferry, M., 1991. A numerical model for buckling and growth of delaminations in composite laminates. Comp. Meth. Appl. Mech. 89, 361–380.

Cox, B.N., Marshall, D.B., 1991. The determination of crack bridging forces. Int. J. Fract. 49, 159–176.

Crisfield, M.A., 1983. An arc-length method including line searches and accelerations. Int. J. Numer. Meth. Engng. 19, 1269–1289.

Drzal, L.T., Madhukar, M.S., 1992. Fiber-matrix adhesion and its effect on composite mechanical properties. IV. Mode I and Mode II fracture toughness of graphite/epoxy composites. J. Compos. Mater. 26 (7), 936–968.

Hutchinson, J.W., Suo, Z., 1992. Mixed mode cracking in layered materials. In: Hutchinson, J.W., Theodore, Y.W. (Eds.), Advances in Applied Mechanics, vol. 28. Academic Press, New York, pp. 63–191.

Hwang, W., Han, K.S., 1989. Interlaminar fracture behaviour and fiber bridging of glass epoxy composite under mode I static and cyclic loadings. J. Compos. Mater., 396–430.

Iwamoto, M., Ni, Q.Q., Fujiwara, T., Kurashiki, K., 1999. Intralaminar fracture mechanism in unidirectional CFRP composites. Part II: analysis. Engng. Fract. Mech. 64, 747–764.

Jain, L.K., Mai, Y.W., 1994. Analysis of stitched laminated ENF specimes for interlaminar mode II fracture toughness. Int. J. Fract. 68 (3), 219–244.

Massabò, R., Cox, B.N., 1999. Concepts for bridged mode II delamination cracks. J. Mech. Phys. Solids 47, 1265–1300.

Rice, J.R., 1968. A path independent integral and the approximate analysis of strain concentrations by notches and cracks. J. Appl. Mech.—T. ASME 35, 379–386.

Robinson, P., Song, D.Q., 1992. A modified DCB specimen for mode I testing of multidirectional laminates. J. Compos. Mater. 26 (11), 1554–1577.

Schapery, R.A., Davidson, B.D., 1990. Prediction of energy release rate for mixed-mode delamination using classical plate theory. Appl. Mech. Rev. 43, S281–S287.

Shu, D., Mai, Y.W., 1993. Effect of stitching on interlaminar delamination extension in composite laminates. Comput. Sci. Tech. 49, 165–171.

Sørensen, B.F., Jacobsen, T.K., 1998. Large-scale bridging in composites: *R*-curves and bridging laws. Composites Part A 29A, 1443–1451.

Spearing, S.M., Evans, A.G., 1992. The role of fiber bridging in the delamination resistance of fiber-reinforced composites. Acta Metall. Mater. 40, 1959.

Storåkers, B., Andersson, B., 1988. Non linear plate theory applied to delamination in composites. J. Mech. Phys. Solids 36 (6), 689–718.

Suo, Z., 1990. Delamination specimen for othotropic materials. J. Appl. Mech. 57, 627–634.

Suo, Z., Hutchinson, J.W., 1990. Interface crack between two elastic layers. Int. J. Fract. 43, 1–18.

Suo, Z., Bao, G., Fan, B., 1992. Delamination *R*-curve phenomena due to damage. J. Mech. Phys. Solids 40 (1), 1–16.